FACULTY
OF MATHEMATICS
AND PHYSICS
Charles University

DOCTORAL THESIS

RNDr. Jakub Škoda

2D structures based on metal phosphonates; relationships between arrangement and properties studied by molecular simulations methods

Department of Chemical Physics and Optics

Supervisor of the doctoral thesis: doc. RNDr. Miroslav Pospíšil, Ph.D.

Study programme: Physics
Specialization: Biophysics, chemical and macromolecular physics

Prague 2019

I declare that I carried out this doctoral thesis independently, and only with the cited sources, literature and other professional sources.

I understand that my work relates to the rights and obligations under the Act No. 121/2000 Coll., the Copyright Act, as amended, in particular the fact that the Charles University has the right to conclude a license agreement on the use of this work as a school work pursuant to Section 60 paragraph 1 of the Copyright Act.

In…..... date..... …....

I would like to thank especially my supervisor doc. RNDr. Miroslav Pospíšil, Ph.D. for friendly and constructive atmosphere and his guide during my doctoral studies, I would like to thank RNDr. Petr Kovář, Ph.D. for his precious experienced tips and help about calculations and also doc. Ing. Vítězslav Zima, CSc., DSc. and his colleagues from University of Pardubice for creative cooperation.

Last but not least, I would like to thank my family and closest friends for supporting me during my whole study at the Charles University.

Title: 2D structures based on metal phosphonates; relationships between arrangement and properties studied by molecular simulations methods

Author: RNDr. Jakub Škoda

Department / Institute: Department of Chemical Physics and Optics

Supervisor of the doctoral thesis: doc. RNDr. Miroslav Pospíšil, Ph.D., Department of Chemical Physics and Optics, Faculty of Mathematics and Physics, Charles University

Abstract: This work deals with the structural analysis of layered zirconium sulfophenylphosphonates and their intercalates with the use of the classical molecular simulation methods. The inner composition of both fully and partially sulfonated layers was determined in agreement with available experimental data, especially chemical analysis, thermogravimetric measurements and X-ray diffraction. The calculations revealed the positions of the water molecules in the planes of sulfo groups which strongly affect the resultant diffraction pattern. Within the zirconium sulfophenylphosphonate layered structure, the arrangements of intercalated species based on optically active dipyridylamine molecules and cations of sodium, copper and iron were solved with the respect to the agreement with experimental results and values of potential energy. In case of the dipyridylamine molecules and its derivatives, the resultant disordered partially row arrangements of the organic molecules in the interlayer were showed to influence the dipole moment of the intercalate. From this point of view, nitro-derivative has been picked out as the most suitable for potential applications. Regarding the intercalated cations, sodium cations take up the space of water molecules next to the sulfo groups while copper and iron cations are distributed in a wide row between the layers of zirconium sulfophenylphosphonates.

Keywords: molecular simulations; layered zirconium phosphonates; intercalation; *N*-(pyridin-4-yl)pyridin-4-amine; Na^{+}, Cu^{2+}, Fe^{3+} cations

Contents

1. Introduction

The knowledge of the structure is essential for developing any new material and analysing and tuning its properties. It is not always possible to deduce all the interesting structural characteristics only with experimental methods, whether because of high expenses for the preparation of the material and for the use of all the experimental methods, or because of their insufficient accuracy and relevant analysing possibilities. For those circumstances, it is useful to combine measured data from experimental methods with suitable data from calculation methods.

Metal phosphonates, especially zirconium phosphonates studied in this thesis, are materials with layered structures difficult to analyse due to their disordered feature. It is therefore highly favourable to use molecular simulations which enable us to obtain the most probable structural arrangement of these disordered materials. Zirconium phosphonate is a material with promising applicable properties described in detail bellow. In addition, the layers can serve as a host matrix and can be used for intercalation of organic and inorganic species to bring or enhance specific properties of the resultant materials. For further development of their application, it is fundamental to study their inner composition.

Classical molecular simulations used in this work for geometry optimization and characterization of partially disordered structures were proved to be a powerful and reliable tool for structural analysis. They are based on minimization of the total potential energy of the system that is described by an empirical force-field. The calculations are combined with the experimentally available data which are used both as a basis of the modelling strategy so as a confirmation of the results. The calculation results include the structure of the optimized model, the total crystal energy, the character and the energies of the interactions between the host matrix and intercalated guest molecules. Furthermore, it is possible to analyse in detail the resultant model and obtain statistical and dynamical information about the structure, such as concentration profiles, structural distributions, dipole moments etc.

The experimental methods used in the presented work are mainly the chemical analysis and thermogravimetric measurements which allow us to determine the structural formulae of the studied material. Next, the X-ray diffraction served us, at first, for determining the crystallographic lattice and crystal symmetry, and in the case of the intercalates mainly for deducing the basal spacing. After the calculations,

the X-ray diffraction pattern is used once again for confirmation of the correctness of the model via the comparison with the calculated one.

This work is focused on structural analysis of intercalates of zirconium phosphonates with sulfophenyl groups which arrangements have not been studied in detail before. In addition, the arrangement of the intercalated optically active molecules and metal cations within the interlayer space of the phosphonates is presented. The combination of the methods of molecular modelling and experimental methods such as X-ray diffraction analysis enabled us to carry out the goals of this work:

- to find and optimize the proper calculation procedure to determine the layered structure of zirconium 4-sulfophenylphosphonate (further denoted as ZrSPhP),
- to build and optimize a detailed structural model of ZrSPhP,
- to use this model as a basis for subsequent calculations of its intercalates,
- to analyse the arrangement of non-linear optical active molecules of *N*-(pyridin-4-yl)pyridin-4-amine (APY2) and its derivatives intercalated into the interlayer space of ZrSPhP,
- to compare the arrangement of ZrSPhP with intercalated cations of sodium, copper and iron with different valencies and to describe the mutual interactions between the host and the guest molecules,
- to show possible structural prediction based on the calculation methods.

2. Phosphate and phosphonate chemistry

2.1. Introduction and brief history

During the early years of the second half of the last century, the great potential of phosphate and phosphonate structures was recognized as well as its layered structure. To understand the principles of their properties it was crucial to analyse their composition and structure which was difficult due to its sparingly soluble nature. After the progress of preparing crystal samples during 1960's, the fundamental crystal structure of phosphate layer was finally solved by Clearfield and Smith when they analysed diffraction data of α-zirconium bis-(monohydrogen orthophosphate) monohydrate crystal (*α*-ZrP) [1, 2]. The results were definitely refined ten years later by Troup and Clearfield who came up with $P2_1/n$ space group and new cell dimensions: a = 9.060 Å, b = 5.297 Å and c = 15.414 Å [3].

During 1970's and 1980's Alberti's and other groups were preparing different types of phosphonates – phosphates' derivatives prepared by replacing the OH group of the phosphate with different functional group. Direct reaction of phosphonic acids with Zr^{IV} resulted in general into the compound $Zr(O_3PR)_2$ where R is an alkyl or aryl group [4]. Their layered structure was definitely recognized but no further inner composition was determined because of very insoluble nature of those structures. It took another 15 years until 1993, when Poojary et al. were successful with determination of the structure of phenylphosphonate $Zr(O_3PC_6H_5)_2$ from limited powder data sets [5]. The deduced structure was indeed layered and similar to that of α-zirconium phosphate having *a* and *b* cell dimensions and *β* angle very similar and differing only (and obviously) in *c* dimension. It was clear that they can serve well as ion exchangers with many future applications, such as catalysis [6, 7], sorption [8], molecular recognition [9], energy storage [10], nanocomposites with polymers [11, 12] or in pharmaceutical research [13].

Beside the zirconium phosphonates – first fully determined phosphonate structure – there are plenty of other metal phosphonates compounds possible, based on divalent, trivalent or four-valent metals or even lanthanides (Zn, Mn, Cu, Ti, …) [14]. Generally, they all keep similar layered structures differing according to the valency of the metals.

The α-zirconium phosphate, see Fig. 1a, is not the unique arrangement of zirconium phosphate layers. Another structure type is the γ-zirconium phosphate, see Fig. 1b. Its layer consists of zirconium octahedra, each of them are bonded to four phosphate tetrahedra. This structure was prepared by Clearfield et al. for the first time back in 1960's [15] and in 1990's structurally determined [16, 17]. The λ-zirconium phosphate, see Fig. 1c, was structurally solved in 1994 [18] and is similar to γ-zirconium phosphate, differing mainly by replacing surface phosphates with anionic and neutral species [19].

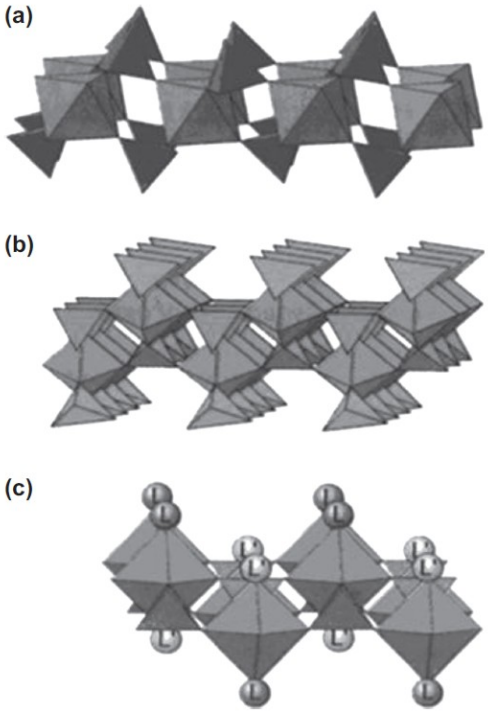

Fig. 1: Schematic structure of most common zirconium phosphates α- (a), γ- (b) and λ-ZrP (c) [19]

2.2. Layers of α-zirconium phosphonates and sulfophenylphosphonates

As mentioned above, the chemistry of the zirconium phosphonates began in 1960's when Clearfield and Smith successfully prepared and characterized a phosphate crystal with the formula $Zr(HPO_4)_2 \cdot H_2O$. During the next decade, its structure was revealed to be consisting of layers built up from the sheets of zirconium octahedra and phosphate tetrahedra, see Fig. 1a [19]. Each zirconium atom is coordinated with six oxygen atoms from six phosphate groups – ZrO_6 octahedra. Three oxygen atoms from phosphate tetrahedra are linked to three different zirconium atoms and the last oxygen atom is protonated and it is the suitable place for bonding ligands in the phosphonate compounds.

The preparation of the zirconium phosphonates is similar to the one for zirconium phosphates – refluxing amorphous or semi-crystalline precipitates or via HF-method [20] which is based on complexation of Zr ions with fluoride anions and slow release of zirconium to dissolved phosphonic acid by a thermal decomposition of the complex.

Structurally, α-zirconium phosphonates are very similar to each other. The common part of the compounds is the inorganic α-ZrP layer while the difference lies in the organic groups which are substituting the -OH phosphatic group. During the last decades, many different zirconium phosphonates were prepared and their characteristics were analysed – carboxy n-alkyl derivative [21], amide and ester derivatives [22], acyl chloride derivative [23], benzene, cyklohexane, alkyl and other organo- derivatives [24], 2-amido ethyl derivative [25] and more recently, epoxy layered zirconium phosphate nanocomposite [26].

From the intercalation chemistry's point of view, the interesting phosphonates are mainly those containing functional groups providing interactions between the host (whole zirconium phosphonate layer) and the guest molecules that enable stable intercalated structures. Because of its strong acidic nature, one of such suitable ligands is the sulfo group (-SO_3H) which strongly interacts with the basic phosphonate layer and is able to produce stable intercalates. Moreover, phosphonates containing sulfo groups were proved to work as proton conductors [27–33]. Materials based on these compounds could be therefore used as components of electrolyte membrane fuel cells [34]. However, the research of their structural properties is still limited due to their high insolubility.

Zirconium sulfophenylphosphonates contain the sulfo groups directly bonded to the phenyl groups. The α-ZrP compounds with the sulfo group in meta position were prepared and described [27, 28]. It was found that it is not possible to prepare pure zirconium 3-sulfophenylphosphonate as it does not precipitate under the reaction conditions. Hence, only these compounds mixed also with phosphate, phosphite and other phosphonate ligands were possible to prepare and to study their conductivity and ion-exchange properties [27, 28].

More recently, the 4-sulfophenylphosphonic acid was synthesized from 4-bromobenzen(ethyl)sulfonate by the reaction with triethylphosphite in the presence of $NiCl_2$ index (the Tavs reaction) [35] and used for the preparation of several metal phosphonates [19, 36–39]. Zirconium 4-sulfophenylphosphonate (ZrSPhP) was prepared with the use of the 4-sulfophenylphosphonic ligand and its protonic conductivity was determined [32].

2.3. Intercalation of non-linear optically active molecules

Intercalation is the chemical or physical process of inserting neutral guest molecules or ions into the interlayer of a solid host lattice without a major change in the arrangement of the host structure. The capability of intercalation is connected with the requirement of strong covalent bonds in the host structure that preservers the unchanged structure during the intercalation reaction and contain accessible vacant sites of suitable size for the guest species to allow intercalation inside the structure [40].

Intercalation can be one way of transferring the selected properties of the guest species from microscopic to macroscopic level. This is the case of APY2 molecule, see its structure in Fig. 2, which is a chromophore that exhibits non-linear optical properties and which is in the centre of interest for applications in signal processing like optical triggering, optical memories, modulators, deflectors or light frequency transducers [41, 42]. APY2 is an example of organic so called push-pull molecule containing donor and acceptor groups. A direct intramolecular charge transfer from an electron donor to an electron acceptor through a system of π-conjugated double bonds causes linear and non-linear optical properties. Based on the behaviour and the modulation of the donor and acceptor parts together with the π-system, molecules' design and tuning of their properties is done [43]. According to that, the second-order susceptibility of the material may be enhanced which is fundamental for applications like optical second harmonics generation [44].

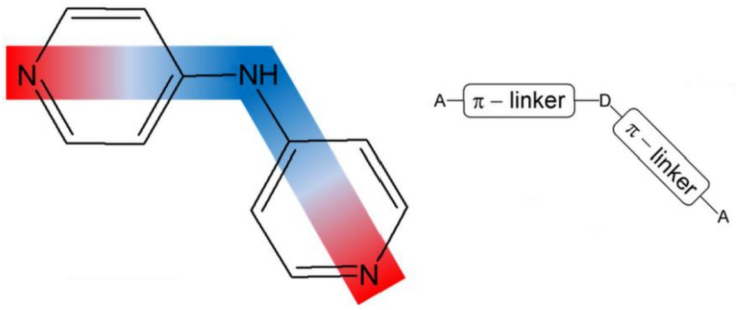

Fig. 2: **APY2** molecule, donor-π-acceptor charge transfer system

It was found that the intercalation of the chromophores into the layered host lattice of ZrSPhP additionally improves their optical properties. The arrangement of the guest molecules of APY2 in the interlayer space between sulfo groups plays the major role in the resultant behaviour of the intercalated structure [43, 45].

2.4. Intercalation with Na^{+}, Cu^{2+} and Fe^{3+} cations

As it was mentioned above, the metal phosphates and phosphonates are materials showing proton conductivity and thus they are perspective for the use in many applications like fuel cells. The proton conductivity and the ion exchange capacity are the main characteristics for such materials. The modification of these layered structures by intercalation is one possible way to improve their properties.

Previously, modifications and intercalations of various types of clay and layered structures of phosphonates by various ions were prepared to achieve or to improve their performance in specific applications – lanthanide ions selective separation [46], catalysts for nitrogen oxides elimination process [47], electrically conducting polymer-clay nanocomposites [48], corrosion inhibitors and biomedical applications [49].

Similarly, for those reasons, the sodium Na^{+}, copper Cu^{2+} and iron Fe^{3+} cations were intercalated into the structure of ZrSPhP. The immersed cations can influence the ion exchange properties and increase the proton conductivity of the resultant material. Determination of the most probable arrangement of the intercalated material in order to understand the behaviour and the mutual interactions of these compounds with the use of classical molecular calculation methods was one of the main tasks of this work.

3. Molecular simulations

3.1. Methods of classical molecular simulations

Molecular simulations are a powerful tool for an optimization of the molecular geometry of large structures containing from hundreds to several thousands of atoms. Opposite to the quantum chemistry methods, classical molecular simulations are based on classical mechanics and the use of the potential energy terms describing the mutual interactions for all atoms and bonds in the calculated model. The set of parameters used in the energy terms are represented by a force-field.

3.2. Force-fields

The force-field is the core of the classical molecular calculations as it expresses the way how each atom in the structure interacts with other atoms around. For each atom, a certain force-field-type is assigned according to its type, bonding character and hybridization. The parameters in each force-field-type cover various information describing the properties and mutual connectivity of the atoms in the system, and bonding and non-bonding interactions, as described below in detail.

The use of a suitable force-field depends on the type of the investigated material. Generally, the force-fields are parametrized using the experimental and/or quantum-mechanical calculations data. For the force-fields based on universal rules, physical properties such as electronegativity, atom radius, atom mass etc. are converted into general force parameters, subsequently used for the calculation. Such force-fields can be used for all atom types in exchange for lower precision of the result. An example of these force-fields is the Universal force field (UFF) [50]. The other class of the force-fields uses the interaction parameters based on experimental data and utilizes the more precise results of quantum chemistry calculations. These force-fields differ by the complexity of the energy terms and by the type of material it was parametrized to. These force-fields can be divided into the first generation force-fields based on empirical observations or simple hybridization rules – Consistent valence force field (CVFF) (used for small organic crystals) [51], Amber (for proteins and nucleic acids) [52], Dreiding (for small organic and inorganic molecules) [53]; and the second generation force-fields with their parameters based primarily on quantum calculations – consistent force field (CFF) (uses bonding

parameters from ab initio calculations and non-bonding parameters from crystal structures) [54], polymer consistent force field (PCFF) (verified by the vibration frequencies and structure arrangement) [55], condensed-phase optimized molecular potentials for atomistic simulation studies force field (COMPASS) [56].

The force-field must contain all the necessary elements for calculations of energy of all atoms in the whole structure:

- a list of force-field types,
- a list of partial charges,
- force-field-typing rules,
- functional forms for the components of the energy expression,
- parameters for the function terms.

The force-field types' parameters are useless without the proper terms that define the total energy hyper-surface as a function of atomic coordinates of all atoms in the structure. Since the atoms are described as dimensionless balls connected by springs with defined elasticity, the forces holding the structure together are determined with the potential energy functions for bonding and non-bonding interactions. The use of proper force-field with suitable and reliable energy functions is the most crucial aspect for a qualitatively precise calculation.

3.3. COMPASS force-field and energy terms

COMPASS force-field represents the second generation force field in the molecular simulations and force-field methods. This force-field is parametrized for a variety of atoms and enables accurate and simultaneous prediction of gas-phase and condensed-phase properties for a broad range of molecules. Its valence parameters and partial atom charges were obtained from ab initio calculations, van der Waals parameters were deduced by fitting the simulated values of cohesive energies and equilibrium densities to experimental data. The derived parameters were subsequently validated for liquids, crystals and polymers.

A set of simple functional forms is used to describe atomic interactions. For different force-fields, these functional forms can vary, even though they describe similar principle. As the COMPASS force-field is the only force-field used for calculations in this thesis, energy terms presented below characterize this force-field.

The complete potential energy can be expressed as a sum of bonding and non-bonding terms:

$$E = E_{bond} + E_{nonbond} \tag{1}$$

3.3.1. Bonding terms

The bonding (valence) potential energy terms corresponding to the interactions via bonds can be divided into several types according to the number of interacting atoms. For two-body interactions, there is a bond-stretching term; for three-body interactions, valence angle deformation term takes place; for four-body interactions, the torsional and inversion terms have to be included. Beside these basic terms, different cross-terms combining the previous ones together are also calculated, as the interactions do not stand out alone but influence each other.

Bond stretching term

The bond stretching term is described just as stretching of a mechanical spring. A good approximation is the harmonic potential, additional anharmonicity is counted with the higher order terms, or for other force-fields, for example, with the Morse potential. The resultant bond stretching term in COMPASS force field is quartic:

$$E_b = \sum_b \left[K_2 (b - b_0)^2 + K_3 (b - b_0)^3 + K_4 (b - b_0)^4 \right] \ , \tag{2}$$

where K_2, K_3 and K_4 are the bond force constants and b_0 is the equilibrium of the bond length b.

Angle bending term

The valence angle bending term is described similarly to the bond stretching, as the elasticity of the spring is represented by the tension between two bonds connected to one common atom, see Fig. 3. Anharmonicity is included the same way as for bond stretching term:

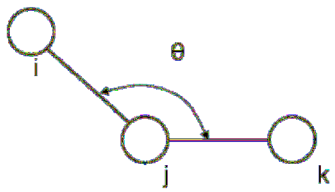

Fig. 3: Angle bending

$$E_\theta = \sum_\theta \left[H_2 (\theta - \theta_0)^2 + H_3 (\theta - \theta_0)^3 + H_4 (\theta - \theta_0)^4 \right] \ , \tag{3}$$

where H_2, H_3 and H_4 are the force constants holding the bond angle θ on the equilibrium value of θ_0.

Torsional term

Torsional term represents the change of the potential energy regarding the rotation around a bond which is described with the change of geometry of four atoms i, j, k and l, see Fig. 4. Such terms must be periodical and usually are calculated as cosine part of the Fourier expansion of the torsional angle, as well as for the COMPASS force-field:

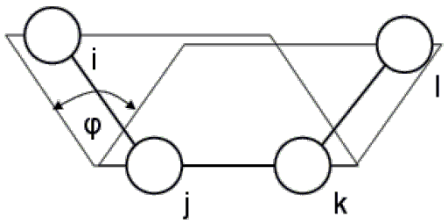

Fig. 4: Torsional angle

$$E_{\Phi} = \sum_{j} \frac{1}{2} B_j \left(1 + \cos\left[n_j \Phi - \Phi_0\right]\right) \quad , \tag{4}$$

where B_j is the height of the rotational barrier around the torsional angle Φ, Φ_0 is the initial phase shift, n_j is the periodicity of the potential function.

Inversion term (out-of-plane deformation)

Inversion term characterizes also the geometry of four atoms and describes their deviation from plane alignment. It is described in different ways, the COMPASS force-field uses an average of three Umbrella terms (for three planes around the atom i):

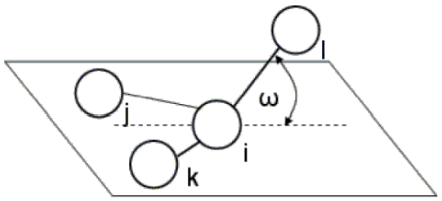

Fig. 5: Inversion angle

$$E_{inv} = \frac{K_{\omega}}{2\sin^2(\omega_0)} \left(\cos\omega - \cos\omega_0\right) \quad \text{for } \omega \neq 0 \tag{5a}$$

$$E_{inv} = K_{\omega}\left(1 - \cos\omega_0\right) \quad \text{for } \omega = 0 \tag{5b}$$

where K_{ω} is the force constant and ω is the angle between the bond i-l and its projection on the i-j-k plane, see Fig. 5, and ω_0 its equilibrium value.

Cross-terms

Cross-terms represent combination of different contributions to the total potential energy since one individual interaction is not separated from the others but they are linked together. These combinations include the mix of the previous terms, thus the stretch-stretch, stretch-bend, torsion-stretch, torsion-bend-bend, bend-torsion-bend and stretch-torsion-stretch terms are formed. For the COMPASS force-field, the terms are expressed in the same order as following:

$$
\begin{aligned}
E_{crossterms} = & \sum_{b,b'} K_{bb'}(b-b_0)(b'-b'_0) + \sum_{b,\theta} K_{b\theta}(b-b_0)(\theta-\theta_0) \\
& + \sum_{b,\phi} K_{b\phi}(b-b_0)[k_1\cos\phi + k_2\cos 2\phi + k_3\cos 3\phi] \\
& + \sum_{\theta,\phi} K_{\theta\phi}(\theta-\theta_0)[k_1\cos\phi + k_2\cos 2\phi + k_3\cos 3\phi] \\
& + \sum_{\theta,\theta'} K_{\theta\theta'}(\theta-\theta_0)(\theta'-\theta'_0) + \sum_{\theta,\theta',\phi} K_{\theta\theta'\phi}(\theta-\theta_0)(\theta'-\theta'_0)(\cos\phi)
\end{aligned}
\quad , \qquad (6)
$$

where the symbols represent the same quantities as for the single interaction terms [56].

3.3.2. Non-bonding terms

Coulombic interaction term

The charges of the atoms cause the electrostatic interaction which is represented by the coulombic term:

$$E_{Coul} = C\frac{q_i q_j}{R} \quad , \qquad (7)$$

where C is Coulomb's constant, q_i and q_j are the charges on the atoms i and j and R is their mutual distance.

As the electrostatic interaction has infinite range, the Coulomb energy must be calculated in an approximate form. One way, used in this work, is the Ewald summation method [57] where the Coulomb term is divided into a real-space sum and a reciprocal-space sum to avoid slow convergence of this term.

van der Waals interaction term

The van der Waals interactions are calculated using the Lennard-Jones potential. Its form varies according to the power of the first attractive part, so that for example 12/6 or 9/6 potentials are created. In COMPASS force-field the latter form is used:

$$E_{vdW} = D_0\left[2\left(\frac{R_0}{R}\right)^9 - 3\left(\frac{R_0}{R}\right)^6\right] \quad , \qquad (8)$$

where R is the inter-atomic distance of an atom couple whose van der Waals energy is calculated, D_0 is the parameter characterizing the depth of the potential well and R_0 is the atomic equilibrium distance. The van der Waals energy is the sum of the interactions of all atom couples closer than defined cut-off distance. To avoid discontinuity of the energy surface, spline functions, defined using quadratic polynomials, are used to continuously depress the interactions [58].

3.4. Minimization algorithms

The primary goal of molecular mechanic simulations is to find the optimized model of the studied structure. The total potential energy is linked with the positions of all atoms in the structure by bonding and non-bonding terms defined by the parameters from the force-field. Thus, the aim of the calculations is to find the minimum of the potential energy for given conformation together with the most probable arrangement of the atoms. Different algorithms are used to minimize the potential energy while changing the geometry of the structure. The most often used algorithm for minimization is *line search* which is based on iterative defining a derivative vector and narrowing the minimum between two points with higher energies. The way how to define new direction to the minimum distinguishes between different algorithms [58].

3.4.1. Steepest descent

The method of steepest descent is usually used as the initial algorithm to find the energy minimum while it is most effective further from the minimum when the gradients are high. In each step, a new direction vector is defined as the descending gradient in the current point of the energy surface. The direction of the new vector is perpendicular to the previous one, which generally does not lead to the minimum. Closer to the real energy minimum, this causes oscillating around the minimum.

The evaluation of the energy terms is the most time-consuming part of the calculation. To safe the calculation time, instead of classical *line-search* of the energy minimum along the gradient vector, a randomly determined point with lower energy compared to the initial value might be used as a subsequent starting point for setting of a new direction. Despite the irregular way to the minimum, the number of iterations remains roughly the same with substantial reduction of time used for energy evaluation.

3.4.2. Conjugate gradient

The method of conjugate gradient is subsequently used after the steepest descent algorithm as it requires atomic configuration closer to the minimum and almost quadratic energy surface to prevent instability of the iterations. Compared to the steepest descent algorithm which always uses an orthogonal direction to the previous one, the conjugate gradient method is based on corrections of the new direction with the use of the previous direction. The algorithm evaluates the energies

in a complete set of conjugate directions. Thus, each subsequent step of the iteration improves the direction toward the energy minimum.

The new direction vector $\boldsymbol{h}_{i+1}$ in conjugate gradient method from the point i+1 is calculated as a sum of the gradient of the energy surface $\boldsymbol{g}_{i+1}$ at that point and previous direction $\boldsymbol{h}_i$ scaled by a constant γ_i:

$$\boldsymbol{h}_{i+1} = \boldsymbol{g}_{i+1} + \gamma_i \boldsymbol{h}_i, \tag{9}$$

where γ_i is a scalar constant that can be defined either as in Polak-Ribière method [59]

$$\gamma_{i_{PR}} = \frac{(\boldsymbol{g}_{i+1} - \boldsymbol{g}_i) \cdot \boldsymbol{g}_{i+1}}{\boldsymbol{g}_i \cdot \boldsymbol{g}_i} \quad , \tag{10}$$

or as in Fletcher-Reeves method [60]

$$\gamma_{i_{FR}} = \frac{\boldsymbol{g}_{i+1} \cdot \boldsymbol{g}_{i+1}}{\boldsymbol{g}_i \cdot \boldsymbol{g}_i} \quad . \tag{11}$$

The calculation time of one iteration step is remarkably higher compared to the steepest descent method because the calculation and storage of the values of the complete set of gradients and directions is necessary and more evaluations of the energy functions are performed. This is compensated by more efficient convergence of this method to the energy minimum.

In Materials Studio modelling environment [58], both types of algorithms can be used during the optimization process. Moreover, the Smart algorithm can be selected which automatically switches between the appropriate algorithm after reaching set criteria.

3.5. Molecular dynamics

Molecular dynamics is the calculation of the time evolution of the system including the positions of all atoms in the structure within the influence of all forces to it. In classical molecular dynamics, the classical Newton equations of motion for a system of atoms which interact according to the force-field are solved.

During the dynamics, the system undergoes various changes in its arrangement and different conformations of the structure can be explored. By the generation of statistical ensembles, see below, thermodynamic variables of the system such as temperature or pressure can be controlled. Various dynamic properties can be subsequently calculated and analysed.

According to the settings of the calculation, molecular dynamics can be used for different applications in chemical simulations. The dynamics calculations allow us to study the motion of atoms, molecules or larger molecule clusters and determine their macroscopic properties such as diffusion coefficients.

3.5.1. Newton's equations

The principle of molecular dynamics is solving Newton's equations of motion for all atoms in the model:

$$-\frac{dV}{d\boldsymbol{r}_i}=m_i\frac{d^2\boldsymbol{r}_i}{dt^2}=\boldsymbol{F}(t) \quad , \tag{12}$$

where V is the potential energy which causes the force $\boldsymbol{F}$ on the atom i with the mass m_i and coordinate $\boldsymbol{r}_i$. This set of equations is deterministic which means that only the initial coordinates and velocities are required to determine the evolution of the system in any later time. The result of the complete dynamics calculation is a set of coordinates and velocities saved in determined times which is called a trajectory. At the beginning of each dynamics calculation, the coordinates are taken from the input file (structural file with the optimized model) and the velocities in the first step are randomly generated corresponding to the statistical distribution for desired temperature related to Maxwell-Boltzmann equation. That is the reason why molecular dynamics calculations cannot be repeated exactly but average values of thermodynamic variables correspond.

3.5.2. Integration algorithm

The solution of the equations of motion can be obtained with the method of finite differences where the known coordinates and velocities of all atoms in the structure at the time t serve to calculate coordinates and velocities at the time $t+\Delta t$. The difference Δt is so called time-step.

The algorithm for solving motion equations is called the integrator whose quality is the limiting factor for the calculation time. The commonly used integrator is the Verlet leapfrog integrator [58] that allows us to use enough long time-step and well preserves the energy of the system under good memory requirements in reasonable time. Moreover, it requires only one energy evaluation per one step. Its only major disadvantage is asynchronized coordinates and velocities during the calculation. The algorithm with given positions $\boldsymbol{r}(t)$, velocities $\boldsymbol{v}(t - \Delta t/2)$ and accelerations $\boldsymbol{a}(t)$ is represented by following equations:

$$\boldsymbol{v}\left(t+\frac{1}{2}\Delta t\right)=\boldsymbol{v}\left(t-\frac{1}{2}\Delta t\right)+\Delta t\,\boldsymbol{a}(t) \quad , \tag{13}$$

$$\boldsymbol{r}(t+\Delta t)=\boldsymbol{r}(t)+\Delta t\,\boldsymbol{v}\left(t+\frac{1}{2}\Delta t\right) \quad , \tag{14}$$

$$\boldsymbol{a}(t+\Delta t)=\frac{\boldsymbol{F}(t+\Delta t)}{m}=\frac{\left(-\frac{dV}{d\boldsymbol{r}_i}\right)_{\boldsymbol{r}(t+\Delta t)}}{m} \quad . \tag{15}$$

The correct choice of the time-step is the key parameter in all integration algorithms. Too large time-step may cause inaccuracy of the resulting trajectory or even instability of the calculation, too small time-step unnecessarily increase the calculation time. Usually, the limit for the time-step is the highest motion frequency between two atoms in the model, i.e. usually vibrational frequency of C-H bond stretching in the magnitude of 10 fs. To satisfy assumption of the algorithm that velocities and accelerations are constant over one step, the integration time-step is set to one tenth of that frequency or lower, for example 0.5-1 fs in this case.

3.5.3. Types of dynamics

In addition to the basic molecular dynamics calculations, there are extended types of dynamics differing in various parameters. Impulse dynamics is useful to overcome energy barriers before relaxing of the structure by assigning explicit initial velocities to selected atoms before the start of the calculation. Quench dynamics consists of a set of geometry optimizations, so called quenches, each of them starting after a certain number of dynamics calculation steps. The dynamics then continues from the pre-optimized structure and both optimized structures and dynamics trajectories are saved into the trajectory files. Simulated annealing dynamics offers changes in temperature interval by repeating of increase and decrease of temperature which is suitable for overcoming energy barriers for trapped structure conformations in local energy minimum and for phase transitions.

The result of the dynamics calculations is saved into the trajectory file. It consists of a set of structural models obtained during the dynamics in regular time intervals and serves for subsequent analysis of dynamic behaviour and parameters of the system such as thermodynamic variables, time dependent processes – diffusion, cell parameter changes, etc.

3.5.4. Statistical ensembles

During the molecular dynamics calculation, the system is following the surface of constant energy. In some cases, like under the exposition to external pressure or exchange of heat with surrounding environment, the energy is not preserved and the dynamics calculation methods must be extended to control the pressure and temperature. Consequently, the statistical ensembles can be generated according to the state variables being kept fixed. From the averages and fluctuations of their values, dynamic and structural information of the system can be deduced.

The NVE ensemble conserves constant energy, volume and number of particles and is known as the microcanonical ensemble. The evolution of the system is obtained by solving the Newton's equations without any control of pressure or temperature. Small fluctuations of the total energy may be caused by computational errors or asynchrony of the integration in case of using Verlet leapfrog algorithm [58]. The temperature is not controlled and can therefore oscillate around its average value according to the change between the potential and kinetic energies, hence, the NVE ensemble is not suitable for equilibrium dynamics.

The NVT ensemble keeps constant temperature, volume and number of particles. It is known as the canonical ensemble and is obtained by controlling thermodynamic temperature by one of the methods described below, except the velocity scaling which does not produce a true canonical ensemble. The NVT ensemble is suitable for the cases when no pressure control is required or for system without periodic boundary conditions where the pressure is not defined.

The NPT ensemble conserves pressure, temperature and number of particles. It is used for controlling the temperature and pressure of the periodic systems as the pressure is adjusted by changing the cell volume.

3.5.5. Temperature and pressure control

The appropriate control of the temperature and/or pressure is necessary to produce required true statistical ensembles for further analysis of the system.

There are several methods of adjusting and controlling the temperature. As one of the most basic state variables, temperature is in microscopic description connected with the kinetic energy of the system and thus with the atomic velocities. The Maxwell-Boltzmann distribution in the equilibrium system of temperature T describes the probability $f(v)$ of the velocity v of an atom with the mass m:

$$f(v)dv=\left(\frac{m}{2\pi k_B T}\right)^{\frac{3}{2}}\exp\left(-\frac{m v^2}{2k_B T}\right)4\pi v^2 dv \quad , \tag{16}$$

where k_B is the Boltzmann constant. The Cartesian components of the velocities v_x, v_y and v_z have the Gaussian distributions, such as

$$g(v_x)dv_x=\left(\frac{m}{2\pi k_B T}\right)^{\frac{1}{2}}\exp\left(-\frac{m v_x{}^2}{2k_B T}\right)dv_x \quad . \tag{17}$$

Thermodynamic temperature is a measure of kinetic energy, they are related via the equipartition theorem that assigns to each degree of freedom an average energy $k_BT/2$. For the kinetic temperature T_{kin} and the kinetic energy E_k the following relation applies:

$$E_k=\frac{N_f k_B T_{kin}}{2}=\sum_{i=1}^{N}\frac{m v_i^2}{2} \quad , \tag{18}$$

where N_f is the number of degree of freedom (3N-6 for non-periodical system, 3N-3 for periodical system, as 3 degrees of freedom for translation of the centre of gravity are not counted and for non-periodical systems also 3 degrees of freedom for its rotation).

During the dynamics calculation, the initially assigned velocities according to the distributions above are changing as the kinetic energy is transferred to the potential energy. Different algorithms are used to keep the velocities to agree with the Maxwell-Boltzmann distribution and to give the correct statistical ensemble, i.e. the probabilities of configurations are according to the statistical laws [61].

Direct velocity scaling is a forced method to achieve requested precise temperature. As effectively this method works, it is not generally used for the simulations because it does not produce correct statistical ensemble and suppress naturally occurring fluctuations. It is used for quick change of temperature to achieve equilibrium state with desired temperature.

Berendsen thermostat can be used for equilibrium state and consists of multiplying each velocity by the factor

$$\lambda=\left[1-\frac{\Delta t}{\tau}\left(\frac{T-T_0}{T}\right)\right]^{\frac{1}{2}} \quad , \tag{19}$$

where Δt is the time-step, τ is the characteristic relaxation time, T_0 is the requested temperature and T is the instantaneous kinetic temperature [62].

Nosé-Hoover's thermostat uses the Hamiltonian of the system with an added fictional degree of freedom for the interaction with the heat bath [63]. Andersen's thermostat is based on influencing the temperature in real time during the simulation. In each step, it changes the velocity of one atom according to the Boltzmann distribution, so it works as a contact statistical heat bath for one atom at the moment [64].

The pressure is defined only for periodical systems where a certain volume of space is occupied. The coordinates of the atoms and the forces between them defines its value. Controlling of the pressure is done by changing of the volume of the system. In Berendsen method, the barostat works with the changes of atom coordinates and the size of the cell, similarly to the Berendsen thermostat, by multiplying of the lattice vector by a factor

$$\mu = \left[\frac{\Delta t}{\tau} \gamma \left(P - P_0 \right) \right]^{\frac{1}{3}} , \tag{20}$$

where Δt is the time-step, γ and τ are parameters of compressibility and relaxation time, P_0 is the requested pressure and P is the instantaneous pressure in the system [62].

In the Andersen method, the volume is added as a variable and is included into the Lagrangian of the system that is used to produce motion equations [64]. In the Parinello-Rahman method, in addition to the previous one, both the size and the shape of the cell can be varied and it is therefore suitable for cases when the changes of cell lengths and angles are required [65].

3.6. Methods of X-ray powder diffraction

Since the very beginning of science itself, to understand the inner structural constitution of matter has been the goal of scientists. The more complex and precise determination of the structure was requested, the more advanced methods were necessary. Higher resolution of those methods enabled scientists to explore the structure in the dimensions of single atoms. One of the most common methods of structural analysis of crystallic materials is the X-ray diffraction (XRD), which explores the regular arrangement of the atoms and determines their types and their positions in a periodic lattice [66].

3.6.1. Basic principles of X-ray diffraction

The diffraction pattern of studied crystallic material is the result of the periodicity of spatial arrangement in the crystal lattice. The resulting quality of the diffraction pattern is linked together with the quality of the prepared crystal. If the structure exhibits impurities, it will be more difficult or even impossible to deduce its inner composition.

If the X-rays are applied and collide with the studied material, they are scattered on the atoms where secondary waves of the radiation are created. As the atoms are regularly ordered in the structure, a regular array of spherical waves is produced. In a few specific directions, a constructive interference is achieved. Thus, the XRD method is based on the measuring of the intensity of the scattered radiation under different angles.

Reciprocal space

The geometric relationships for diffraction patterns are described in the reciprocal space. It is derived from the real space by building a reciprocal lattice with its axes orthogonal to the real space lattice's axes. Each sequence of those planes are denoted with numbers h, k, l, so called Miller indices, that characterize the number of segments that are created by division of the crystallographic axes $\boldsymbol{a}$, $\boldsymbol{b}$, $\boldsymbol{c}$ by those planes. The reciprocal lattice's points are marked in the distance $1/d_{hkl}$ from the origin of both real and reciprocal lattices where d_{hkl} is the distance between two adjacent planes. Therefore, each point in the reciprocal lattice corresponds to a set of lattice planes in the real space. It can be represented by the lattice vector

$$\boldsymbol{G}_{hkl} = h\boldsymbol{a}^* + k\boldsymbol{b}^* + l\boldsymbol{c}^*, \tag{21}$$

where $\boldsymbol{a}^*$, $\boldsymbol{b}^*$ and $\boldsymbol{c}^*$ are the basic translation vectors of the reciprocal lattice.

Laue diffraction equations

When the diffraction is reached, an arrangement of atoms in the crystal with periodicity a scatters incident radiation with the wavelength λ so that the path difference of the rays is integral multiple of the wavelength:

$$\boldsymbol{a}(\boldsymbol{s}-\boldsymbol{s}_0)=h\lambda \quad , \tag{22}$$

where $\boldsymbol{s}$ and $\boldsymbol{s}_0$ are the unitary vectors in the direction of scattered and incident rays and h is an integer. Such relations must be satisfied in all three dimensions at the same time, so for the set of atoms with the periods $\boldsymbol{a}$, $\boldsymbol{b}$, $\boldsymbol{c}$ it means:

$$\begin{aligned} \boldsymbol{a}(\boldsymbol{s}-\boldsymbol{s}_0)&=h\lambda, \\ \boldsymbol{b}(\boldsymbol{s}-\boldsymbol{s}_0)&=k\lambda, \\ \boldsymbol{c}(\boldsymbol{s}-\boldsymbol{s}_0)&=l\lambda. \end{aligned} \tag{23}$$

These three relations are called Laue diffraction equations. For different *h*, *k*, *l,* at most one diffraction direction ***s*** satisfies those conditions.

Ewald's sphere

The quantity $(\boldsymbol{s}-\boldsymbol{s}_0)/\lambda$ is called diffraction vector. If it is identical with a lattice vector $\boldsymbol{G}_{hkl}$, the diffraction occurs:

$$\frac{\boldsymbol{s}-\boldsymbol{s}_0}{\lambda}=\boldsymbol{G}_{hkl} \quad . \tag{24}$$

It can be clearly shown via the Ewald's sphere construction, see Fig. 6. Ewald's sphere is a sphere with a radius $1/\lambda$ with the studied crystal in its centre. The origin of the reciprocal space is in the point of the sphere where the incident ray is leaving the sphere. If a lattice point *hkl* lies on the surface of the sphere, the equation (24) as well as the Laue diffraction conditions are satisfied and the diffracted ray goes through this point. The diffraction pattern is therefore an image of the reciprocal lattice of the crystal.

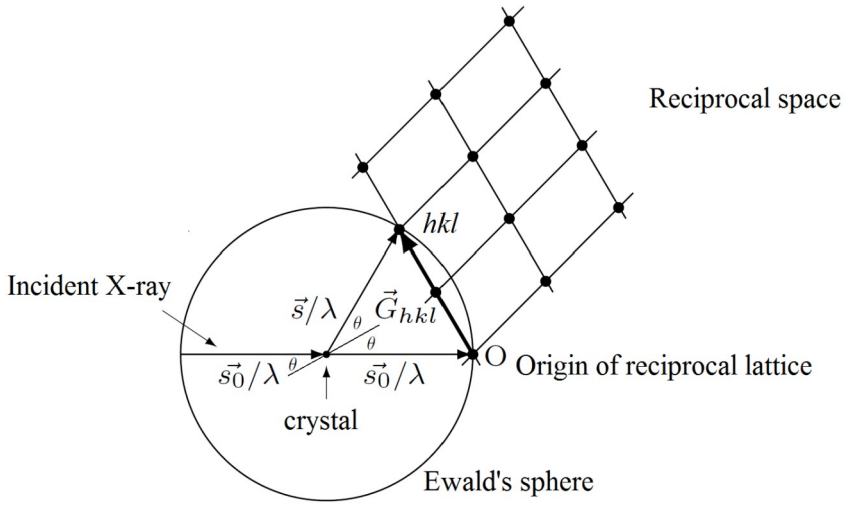

Fig. 6: Ewald's sphere construction

Bragg's law

When the Laue equations are satisfied, the diffraction vector $\boldsymbol{G}_{hkl}$, that also defines the diffraction angle 2θ, is perpendicular to corresponding *hkl* planes. The half of the diffraction angle is called Bragg's angle θ, see Fig. 6. For this angle, it stands:

$$\sin\theta=\frac{|\boldsymbol{G}_{hkl}|/2}{1/\lambda} \quad , \tag{25}$$

and considering that the magnitude of the diffraction vector is reciprocal the distance of *hkl* planes $|\boldsymbol{G}_{hkl}| = 1/d_{hkl}$, we get the Bragg's law:

$$2\,d_{hkl}\sin\theta = n\,\lambda \quad , \tag{26}$$

where n is the order of the diffraction.

3.6.2. Calculating X-ray diffraction patterns

For calculating the resultant diffraction pattern, the intensities for all diffraction angles must be calculated. An essential ingredient for this is the calculation of the structure factors F_{hkl} which are related to the atomic positions of N atoms and their atomic scattering factors via equation

$$F_{hkl} = \sum_{1}^{N} f_n e^{2\pi i(h u_n + k v_n + l w_n)} \quad , \tag{27}$$

where u_n, v_n and w_n are fractional coordinates of n-th atom and f_n is the atomic scattering factor. The final powder diffraction intensity observed under the diffraction angle is then given as

$$I(\theta) = \sum_{hkl} p_{hkl}(2\theta - 2\theta_{hkl}) I_{hkl} = \sum_{hkl} p_{hkl}(2\theta - 2\theta_{hkl}) M_{hkl} P_{hkl} L_{hkl} |F_{hkl}|^2 \quad , \tag{28}$$

where p_{hkl} is profile function used to describe instrumental broadening, I_{hkl} is the integrated Bragg intensity, M_{hkl} is the multiplicity of the reflection *hkl*, P_{hkl} is preferred orientation correction and L_{hkl} is Lorentz and polarization correction for the reflection *hkl* [58].

3.7. Materials Studio modelling environment

Materials Studio is a software for modelling and simulating the relationships of materials' atomic and molecular structure with description of its properties and behaviour. Materials Studio version 4.3. was used for all modelling and all calculations in this work [58].

The user interface, see the Fig. 7, is based on the graphical window for displaying the studied structure. The tools buttons enable to create, handle and visualize the structure in the desired way. The side panels serve for controlling the properties of the structural elements like atom types, bond lengths, charges etc. Other tools serve the user for example for controlling constraints such as fixed positions of atoms, fixed cell parameters, assigning of rigid motion groups etc. Also it is possible to manually set the value of atomic charges as well as to assign them automatically from the appropriate force field. On the bottom of the user interface, the current

calculation's progress is displayed in terms of the percentage of maximal number of iteration steps. The calculation ends either after reaching this number or after satisfying the condition of convergence for the value potential energy.

A number of different modules are available for the specific tasks. The essential calculation engine modules are used for geometry optimization and dynamics calculations, such as Discover or Forcite. In this work, Forcite module was used for all calculations. The module includes all necessary options for the correct setting of the parameters for geometry optimization and dynamics calculations and also for subsequent analysis of the resultant models, such as bond lengths and angles distributions, concentration profiles, mean-square displacement, dipole auto-correlation function etc. Reflex module enables calculating and operating with diffraction patterns and enables us to use refinement methods [58].

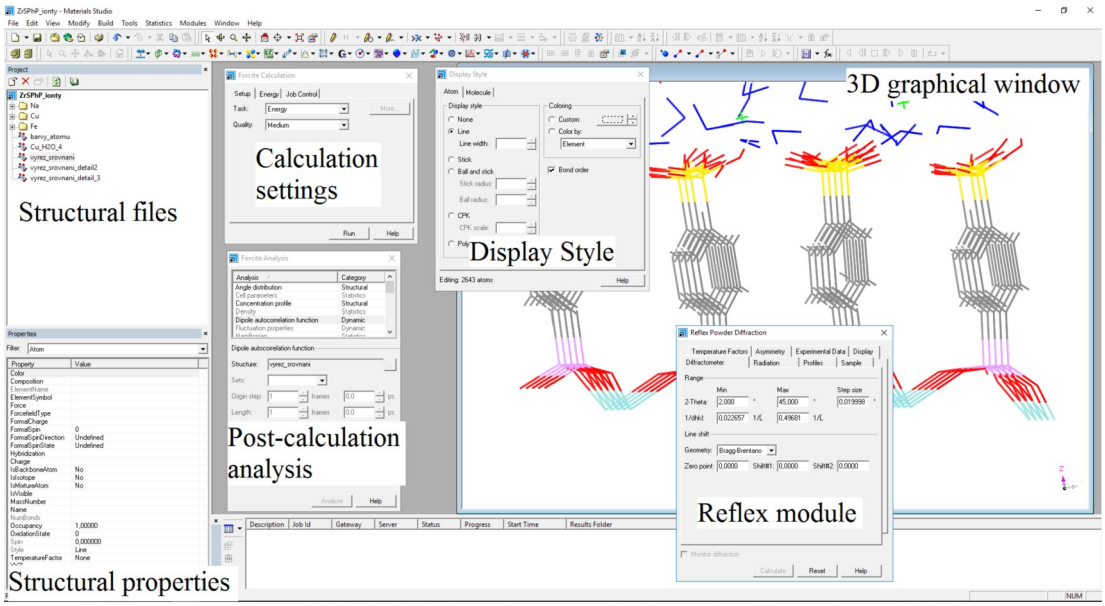

Fig. 7: Materials Studio modelling environment – user interface and basic tools

4. Results and discussions

4.1. Strategy of modelling and calculations

All calculations of ZrSPhP in this work were done in the Materials Studio modelling environment [58] in the calculation module Forcite. The COMPASS force-field [56] was used for all geometry optimizations and dynamics calculations, the space group was set to P1 for the calculation purposes. The electrostatic energy was calculated using the Ewald summation methods [57] and the van der Waals energy was calculated using the atom-based method using the Lennard-Jones potential with cut-off 12 Å and spline 1 Å. Charges were assigned by the force-field. In the case of ZrSPhP intercalated with cations and APY2 and its derivatives, the charge was balanced to reach totally neutral supercell. In the case of APY2 molecules intercalated into ZrSPhP structure, the Qeq method was also used to calculate charges [67]. The resultant models were chosen according to the minimal value of total energy and to the agreement with experimental XRD data.

4.1.1. Preparation of the initial model

The primary goal of all molecular simulations is to obtain the most probable arrangement of the structure using available data from experimental measurements. The experimental data are used in two ways. At first, they serve as initial parameters for building of the initial models of the studied structure. For example, the intensity of diffractions characterizes the positions of the atoms in the structure, diffraction peaks' positions characterize interlayer distances in a layered material, the amount of water molecules and intercalates is taken from thermogravimetric measurements and chemical analysis, etc. At second, after the calculations, the best optimized model is compared with the experimental results.

In the case of ZrSPhP, the initial model was built based on the presumption that its inorganic part is isostructural with the structure of pure zirconium phosphate α-ZrP. The atom coordinates were taken from the refined structure deduced from X-ray diffraction by Troup [3]. This initial model was confirmed to agree with the one described by Čapková et al. [68].

The final part of the initial model's preparation was bonding sulfophenyl molecules to the inorganic layers. The sulfophenyl molecule was built and optimized with the sulfo group in para- position and one sulfophenyl molecule was bonded to

each phosphorus atom in the α-ZrP structure, giving rise to the phosphonate compound. A $5a \times 5b \times 1c$ supercell was built to consider both sufficiently low forced periodicity and reasonable time-consumption of the simulations.

4.1.2. Geometry optimization of ZrSPhP

The optimization process itself was divided into several steps that were found out to approach the desired results.

- At first, the sulfophenyl groups were assigned as rigid motion units, that means that atoms included in such units were not able to move mutually but could change their coordinates only as a group. Thus, the phenyl rings were able to achieve their ideal arrangement with respect to each other. The zirconium phosphate layer was kept fixed during this stage of optimization.
- After that, each α-ZrP layer together with all adjacent phenyl rings and sulfur atoms were assigned as a big motion group, while oxygen and hydrogen atoms of the sulfo groups were kept free to move during the optimization.
- In the third step, the water molecules were added into the structure of the optimized anhydrous ZrSPhP. Various arrangement of the water molecules were tested and compared. The amount of water within the structure was varied slightly around the experimentally deduced value. The precision of the water content analysis is highly dependent on the air humidity and its real value can change significantly.
- The models of the structure with partially sulfonated phenyl rings were prepared by removing sulfo groups and their replacement by hydrogen atoms with appropriate bond lengths. The sulfo groups being deleted were chosen randomly to be evenly distributed along their original layer. Different distributions of deleted sulfo groups, both within the same layer and within the adjacent layers, were prepared and optimized. Models with deleted sulfo groups conjugated in clusters were also studied. However, diffraction of such optimized structures did not show good agreement with the experimental diffraction data and thus they were ruled out from considerations.

Between each of those steps, one procedure of the geometry optimization was performed. For each step, a various set of slightly different initial models were prepared differing in the geometry and positions of the molecules in the structure, for

example in the rotation of phenyl or sulfo groups or in the position of water molecules.

The main task of this part was to reveal the inner arrangement of the structure of ZrSPhP with general formula $Zr(HO_3SC_6H_4PO_3)_x(C_6H_5PO_3)_{2-x}\cdot yH_2O$, where x = 0.7–2. Three main structures were prepared. At first, models with x = 2 (further denoted as ZrSPhP2) were calculated, both hydrated (y = 2) and dehydrated (y = 0) compounds. After that, by deletion of appropriate amount of sulfo groups, the models with x = 1.3 (ZrSPhP1.3) and x = 0.7 (ZrSPhP0.7) were prepared and optimized with various distributions of absenting sulfo groups and with varying amount of water content (y = 2.5–3.5).

4.1.3. Intercalated models

The optimized structure of ZrSPhP2 was subsequently used for further intercalation with optically active molecules APY2 (see Fig. 2) and its 3-methyl- (further denoted as MeAPY2) and 3-nitro- (NO2APY2) derivatives, see Fig. 8. Moreover, the same host structure was used for another modification and intercalation with sodium, copper and iron cations. The cell parameter *c* was enlarged for the initial models of intercalated structures to approximately agree with the experimental basal spacing obtained by XRD.

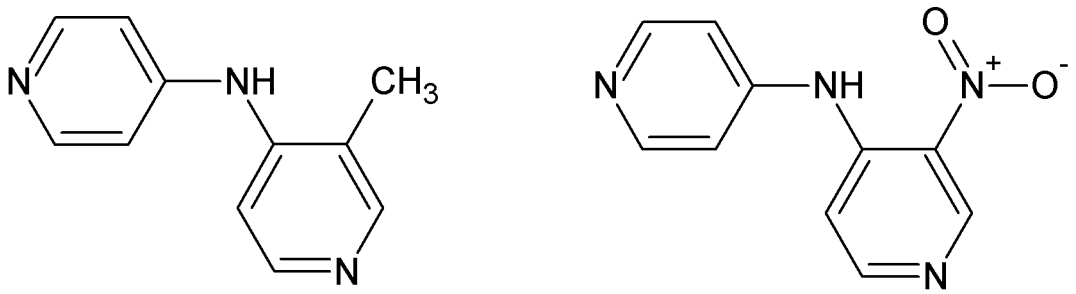

Fig. 8: Structural formulae of intercalated derivatives 3-methyl-APY2 (MeAPY2) and 3-nitro-APY2 (NO2APY2)

Regarding the case of intercalation with APY2 and its derivatives, the experimental analysis of the intercalated material revealed the appropriate amount of 24 optically active molecules of APY2 that were inserted between each of ZrSPhP layers together with 75 molecules of water. The experimental measurements of an absorption spectra indicated protonation of APY2 molecules, hence two hydrogen atoms were bonded to each APY2 molecule and the total charge of each such molecule was set to +2 el. To compensate the total positive charge of the guest molecules, 48 hydrogen atoms were deleted across each ZrSPhP layer and the layer's

charge was set to -48 el. The total composition of the whole supercell was $Zr_{100}(HO_3SC_6H_4PO_3)_{200}^{-96}(APY2)_{48}^{+96}\cdot 150H_2O$. For the APY2 derivatives, chemical analysis detected only 70 water molecules in the calculated supercell.

Two basic initial arrangement types of APY2 molecules were prepared and compared – molecules oriented in the same way and oriented alternately, according to the direction that the central nitrogen atoms were facing. The geometry optimization was then performed followed by Quench molecular dynamics. NVT statistical ensemble was used, temperature was set to 300 K, Berendsen thermostat was used. The time step was set to 1 fs and 10^6 steps were carried out. Analogous procedures of structure optimizations were performed for the MeAPY2 and NO2APY2 derivatives intercalated between the layers of ZrSPhP.

In the case of the MeAPY2 derivative, the protonation was also implied from the experiments, see Fig. 9A. Thus the intercalated molecules were prepared in similar way as for the original molecule of APY2. Regarding the NO2APY2 derivative, the protonation was not clear from the absorption spectra – see Fig. 9B. It seemed that only a part of the intercalated molecules may be protonated [45]. For that reason, both non-protonated and protonated variants were prepared and optimized. Moreover, models with a mix of non-protonated and protonated intercalate and models with single-protonated molecules were studied.

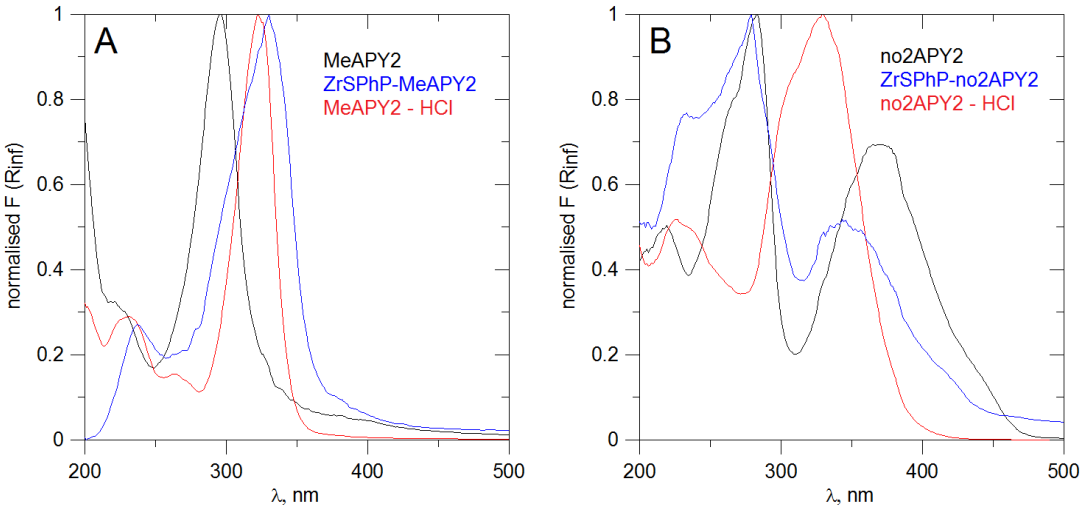

Fig. 9: UV/VIS absorption spectra of A) MeAPY2 and B) NO2APY2 derivatives before and after intercalation into ZrSPhP and after protonation in HCl vapours [45]

Similarly, the metal cations of sodium, copper and iron with different valency were intercalated into the structure of ZrSPhP. Their amount was determined by chemical analysis after the synthesis of the material. For each cation, different

number of hydrogen atoms had to be deleted from the sulfo groups of ZrSPhP, according to their determined chemical formulae. This amount of deleted hydrogen atoms was equal to the number of appropriate cation multiplied by its valency. In the case of sodium, all hydrogen atoms from sulfo groups were deleted, for copper and iron cations only part of the hydrogen atoms were deleted in order to compensate the total charge of the structure. The deletion was done evenly across the layers.

Refinement of the cell parameters *a* and *b* (using the refinement method in Materials Studio with fixed atoms [69]) was used for the models intercalated by cations as well as for the ones with the APY2 and its derivatives. This was done because the non-basal peaks in the calculated diffraction pattern before the refinement were shifted compared to peaks' positions in the experimental diffraction pattern. The choice of the cell dimensions influences the positions of diffraction peaks and it is therefore parameter that is possible to optimize. After the cell refinement, the models were optimized with *c* cell parameter kept free.

4.2. Resultant structure of zirconium sulfophenylphosphonates

The calculated basal spacing of the hydrated model for the fully sulfonated structure ZrSPhP2 was determined to d_{calc} = 20.00 Å, which is in a good agreement with the experimental value d_{exp} = 19.96 Å. The phenyl rings in the optimized structure are slightly tilted at the deviation about 5° from the plane of zirconium phosphate layer and rotated significantly at about 30° along the *z* axis, see Fig. 10. The almost no difference between experimental basal spacings of hydrated and dehydrated model (0.06 Å) served for deducing the proper position of water molecules in the hydrated model. The water molecules may not be located in the middle of the interlayer space but are more likely present in the sheets of sulfo groups, forming a net of hydrogen bonds in these sheets as well as to the opposite sheet of sulfo groups. The hydrogen bonds net is the probable reason for high proton conductivity of this material.

For the dehydrated model, no structural changes were observed except the above mentioned small decrease of basal spacing and smaller amount of hydrogen bonds between the opposite sheets of sulfo groups.

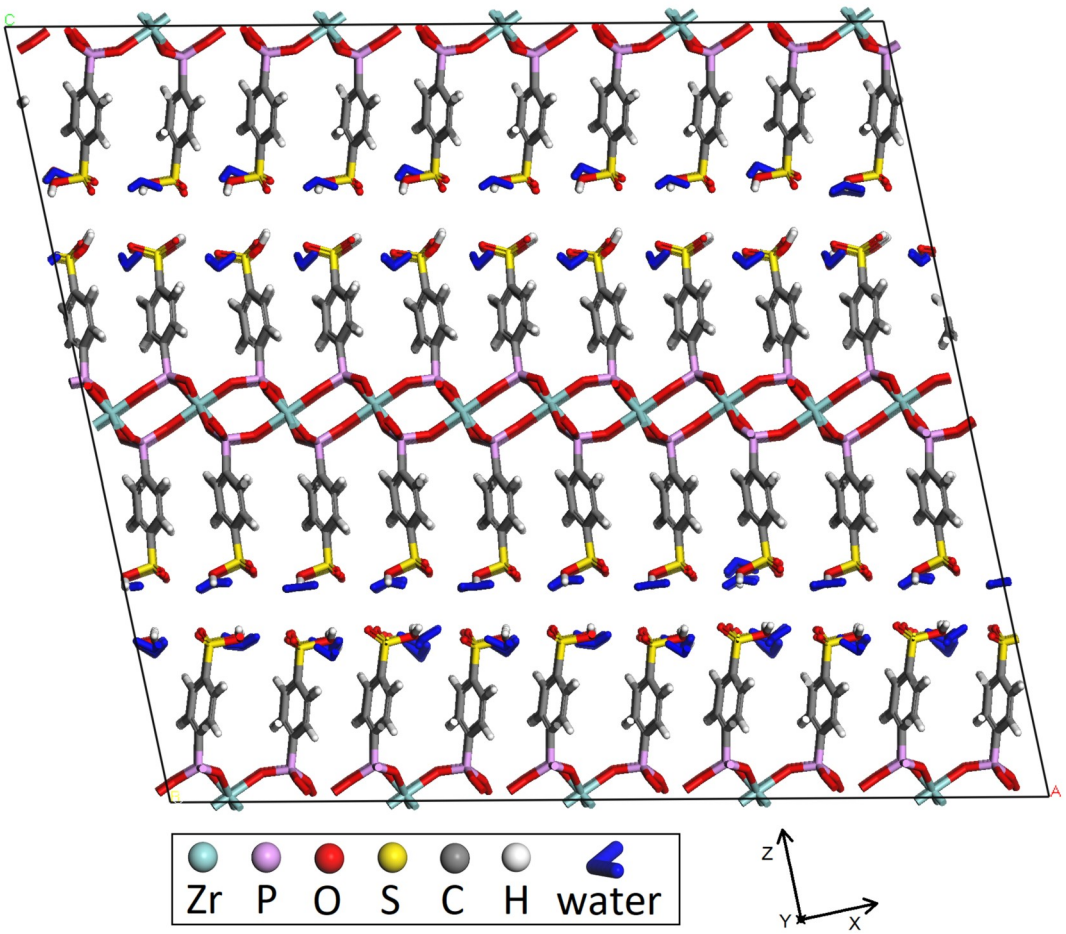

Fig. 10: Resultant optimized structure of ZrSPhP2, side view

The resultant models were chosen according to the value of potential energy and agreement between the calculated and the experimental XRD pattern from a set of tens of calculated models. Very good agreement was reached especially for basal peaks for both hydrated (see Fig. 11) and dehydrated model. The intensity of the second peak is highly influenced by the amount and position of water molecules and confirms once again the correctness of the optimized model. All non-basal peaks can be assigned to the peaks in the experimental pattern. For some of them, the intensity ratios and shape slightly differ which is the result of non-perfect crystallinity of the experimentally prepared compound exhibiting in contrast to the calculated sample with ideal periodic structure.

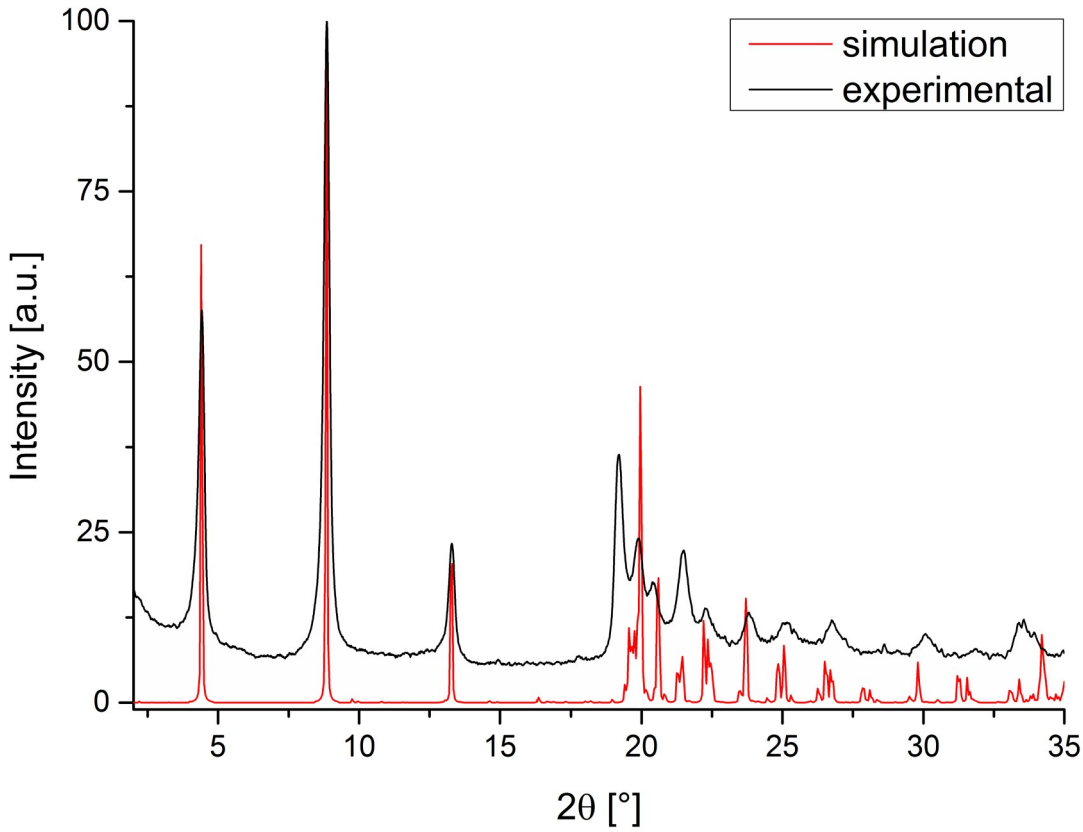

Fig. 11: Comparison of calculated and experimental XRD patterns for ZrSPhP2 [70]

Partially sulfonated ZrSPhP1.3 and ZrSPhP0.7 models were studied with some of the sulfo groups replaced by the hydrogen atoms. The calculations showed that these samples can not contain large clusters of sulfo groups vacancies as such models exhibit completely different diffractions. On the other hand, the model with even distribution of sulfo groups' vacancies along the whole structure did not reach good agreement with experiment either and tended to increase its basal spacing during the optimization. The best match was achieved for models with a small difference around 20 % in the amount of sulfo groups' vacancies in the opposite sulfo sheets. This could be explained by the higher bonding potential that can be created by sulfo group–water molecule pairs from the opposite layers.

4.3. The arrangement of APY2 derivatives within zirconium sulfophenylphosphonates layers

Molecular simulations allowed to determine the arrangement of APY2 and its derivatives within the interlayer of previously optimized structure of ZrSPhP2. Based on the size of the APY2 molecule and its derivatives together with the experimentally determined basal spacings of intercalated structures, a set of models with different

initial arrangements was prepared to satisfy the spatial requirements, i.e. to fit the appropriate amount of the intercalate between the layers of ZrSPhP.

For each prepared and geometrically optimized model, dynamics calculations were performed with parameters described above. The final model exhibits very good agreement between experimental and calculated diffraction patterns, see Fig. 12 The intercalated APY2 molecules prefer monolayer arrangement with the molecules perpendicular to the host layer, see the resultant model with APY2 intercalate in the Fig. 13. The intercalated molecules are arranged mainly parallelly with respect to the layers, some of them are tilted around the *a* axis. From the top view, the APY2 molecules rearranged from the initial fully regular row arrangement to semi disordered one with apparent remains of the rows. The disorder is mainly caused by the interactions between the guest molecules, by the spatial restrictions and the shape of the molecules and also due to the interactions between the host layers and the guest molecules. The water molecules are located in the interlayer space, most of them together with the APY2 molecules are forming a hydrogen bond net between the sulfo groups of the opposite layers.

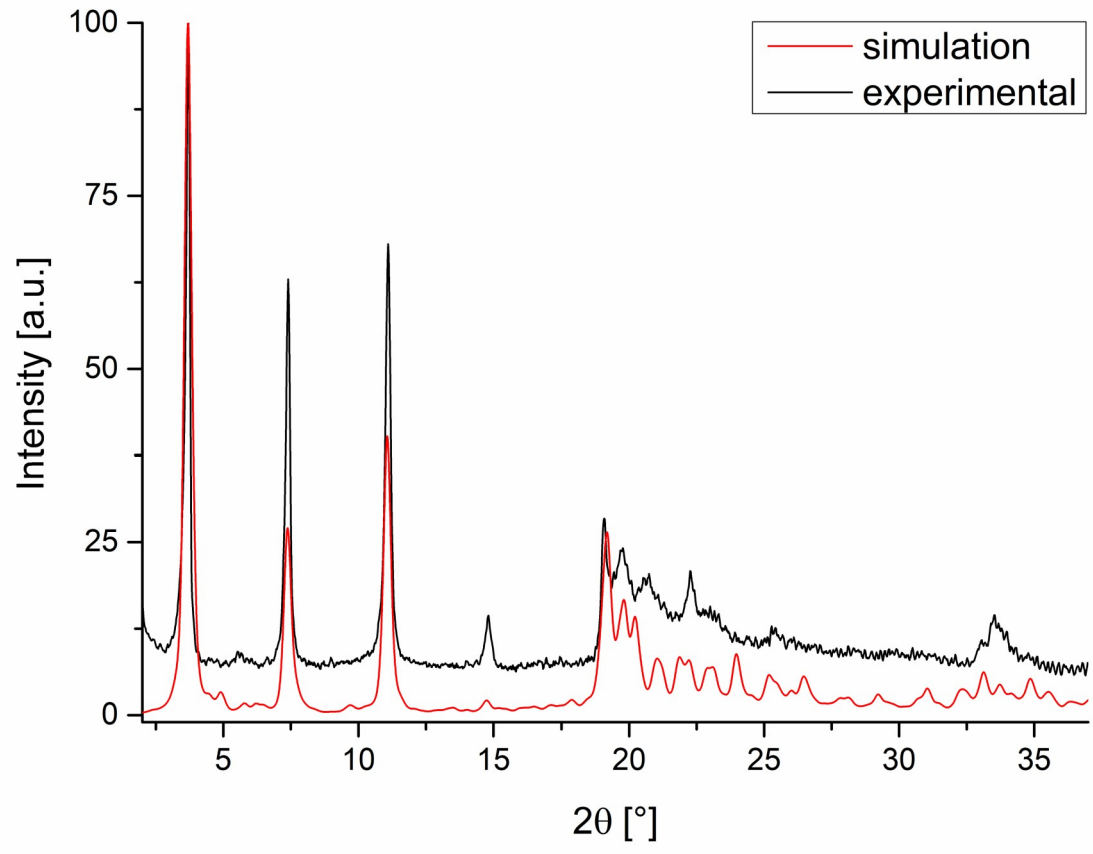

Fig. 12: Comparison of calculated and experimental XRD patterns for ZrSPhP2 intercalated with APY2 molecules [45]

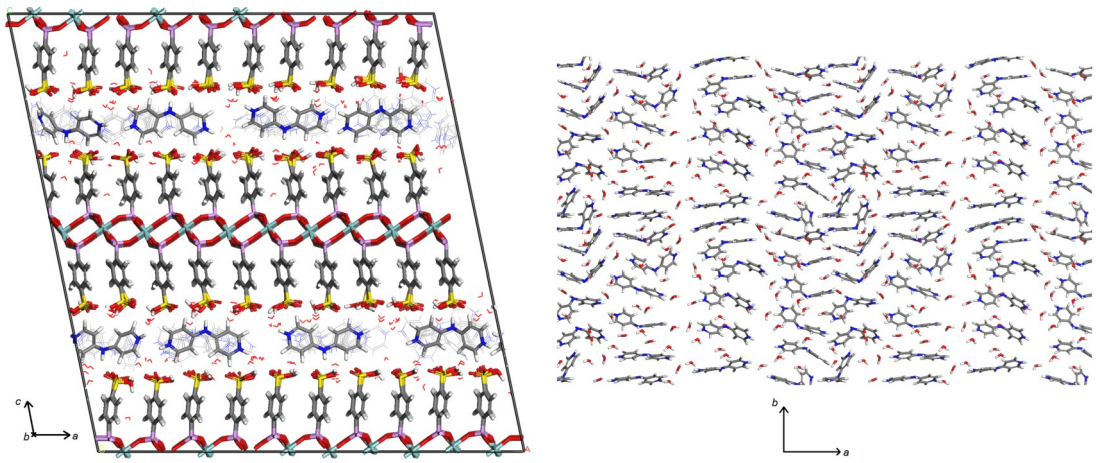

Fig. 13: The optimized arrangement of APY2 molecules within the layers of ZrSPhP2 from side view (left) and top view (right) [45]

Regarding the results of structural optimization of MeAPY2 derivative, the arrangement of the intercalate was much more distributed compared to the APY2's model, see Fig. 14. There is not evident the row ordering built in the initial model like in the case of APY2 intercalate. From the side view, the molecules are more disordered in the interlayer although they possess the same orientation of the individual molecules with respect to the direction of the central nitrogen atom.

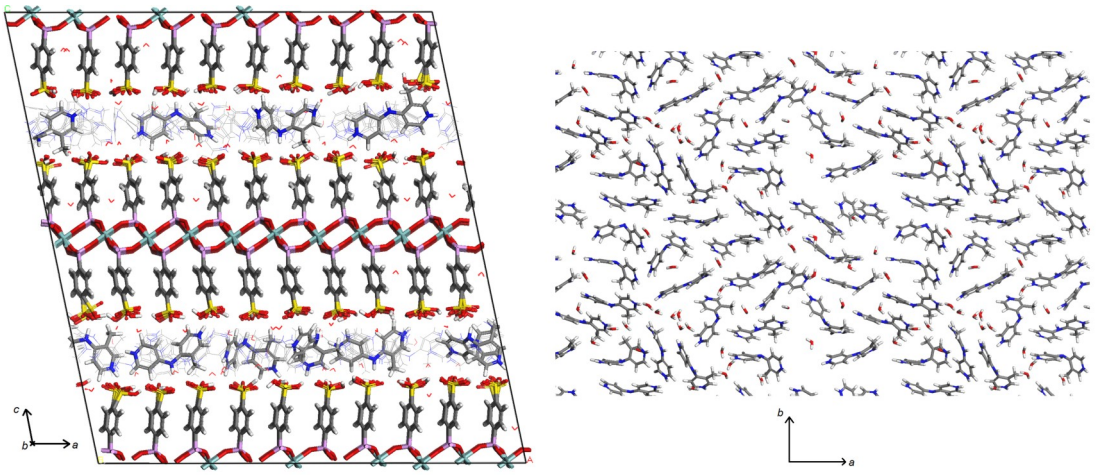

Fig. 14: The optimized arrangement of MeAPY2 molecules within the layers of ZrSPhP from side view (left) and top view (right) [45]

As mentioned above, in the case of NO2APY2 derivative, there were prepared another models containing unprotonated and partially protonated intercalated molecules as the experimental measurements revealed possible partial protonation. The protonation changed also the charge of the intercalated molecules and therefore significantly influenced the mutual interactions between the host layers and the guest. However, according to the calculation results, the best match of basal spacings with experimental values and the best agreement of diffraction patterns was reached for the protonated model, similarly to the APY2 and MeAPY2 intercalates.

The unprotonated and partially protonated models resulted with larger basal spacing values due to weaker mutual interactions between the ZrSPhP and intercalated molecules. The best optimized model of the protonated intercalate, see Fig. 15, contains NO2APY2 molecules with high disorder in the interlayer, but still keeping slight row ordering remaining from the initial model.

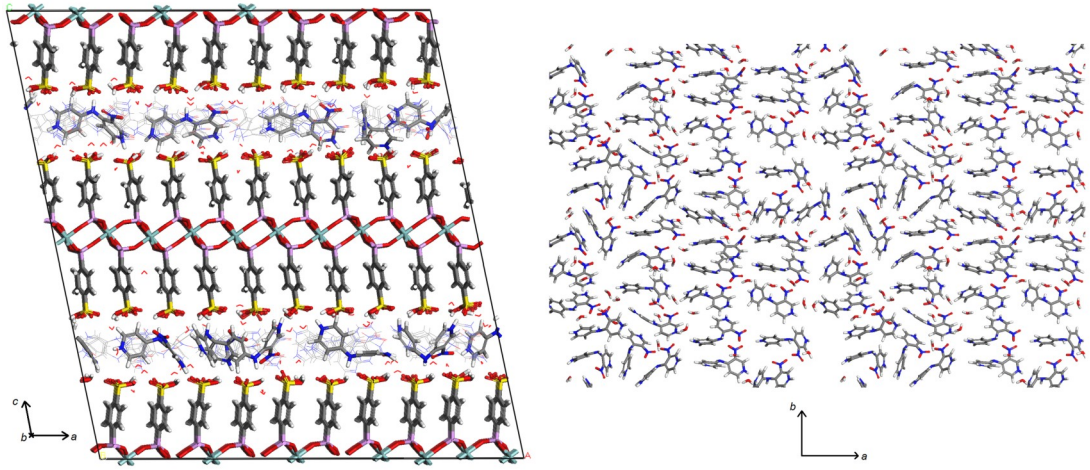

Fig. 15: The optimized arrangement of NO2APY2 molecules within the layers of ZrSPhP from side view (left) and top view (right) [45]

In order to characterize the structures from the point of view of their applications in non-linear optics, dipole moments of all three types of intercalates were calculated as it is a magnitude connected with optical properties of the compound. For each intercalate, symmetrical and asymmetrical arrangements of the molecules were also studied. On the other hand, regarding the APY2 derivatives, NO2APY2 model exhibits much higher total dipole moments of the guest molecules compared to the APY2 intercalate and MeAPY2 derivative. Based on this calculation, NO2APY2 derivative was marked as a promising material for non-linear applications.

4.4. Zirconium sulfophenylphosphonates intercalated with cations

The intercalated structures of ZrSPhP with sodium, copper and iron cations were experimentally synthesized. Molecular simulations methods can describe the influence of the intercalated metal cations on the structure of the ZrSPhP and a mutual arrangement of the layers, sulfo groups, water molecules and guest cations. The structure of ZrSPhP from previous research served as the basic model for further modifications to agree with the formula from chemical analysis $Zr(HO_3SC_6H_4PO_3)_{1.8}(C_6H_5PO_3)_{0.2}$. Three types of cations – Na^+, Cu^{2+} and Fe^{3+} – were inserted into the interlayer space of this modified model according to our previous

calculation procedures (random deletion of sulfo groups) and the experimentally deduced structural formulae.

We obtained a good agreement in basal spacings but non-basal peaks were slightly shifted. Despite of testing of tens different initial models, which differed in the arrangement of the cations and water molecules, we did not reach satisfying agreement of non-basal peaks between the calculated and experimental diffraction pattern after geometry optimization.

Based on these results, cell parameters refinement procedure with fixed atoms was used in order to improve this disagreement. After the refinement procedure, another round of geometry optimization and molecular dynamics was performed. This procedure combined of two cycles of optimization and cell refinement lead to much better agreement, both for basal and non-basal peaks in the diffraction patterns. The models characterized by the lowest energy and the best agreement between the calculation and experiment were chosen as the final structures.

The resultant models showed the differences for three types of cations, see Fig. 16. The sodium cations inside the ZrSPhP layers are distributed regularly and replace mainly the hydrogen atoms of the sulfo groups. They are coordinated between the oxygen atoms of sulfo groups from the same sulfo sheet. The water molecules are distributed between the opposite layers and form a hydrogen bonds' bridge between them.

Copper cations are arranged in a different way – compared to sodium they are positioned mainly between the opposite sulfo sheets and forming wide sheet of cations. The copper cations are located mostly in the way that several oxygen atoms of the sulfo groups from both sheets are deviated from the original positions and coordinated to the cations. Water molecules are disposed around the cations also between the layers, contributing to the coordination of the cations.

Iron cations are intercalated in a much lower amount but possess higher charges. The individual cations are more separated from each other and are evenly distributed in the centre of the interlayer, coordinated more closely to the oxygen atoms of the sulfo groups of both opposite sheets and to the higher amount of water molecules around.

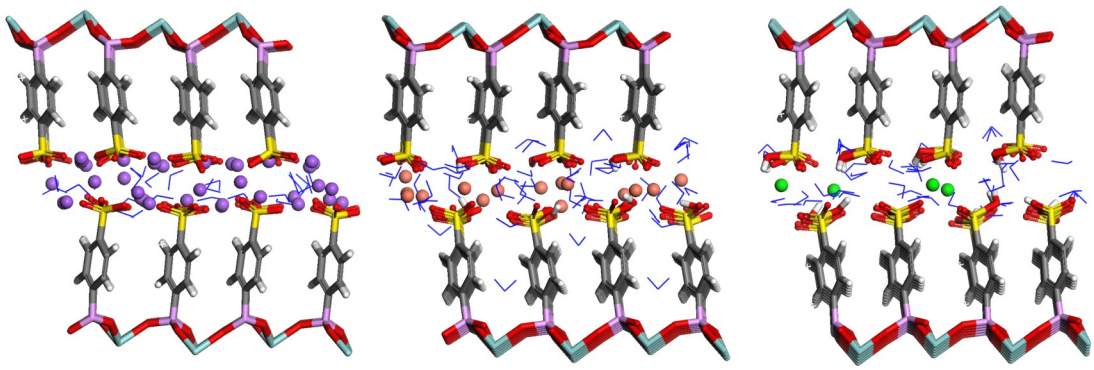

Fig. 16: Comparison of the arrangements of intercalated cations of Na^{+}, Cu^{2+} and Fe^{3+} within the layers of ZrSPhP [69]

For all three types of cations, Connolly surfaces were calculated to compare the final models. Connolly surfaces characterize free volume accessible for the solvent by moving a probe sphere along the van der Waals surface of all atoms, in our case the sphere's radius was 1 Å. The calculated free volumes increase with the valency of the cations: 4070 $Å^3$ for Na^{+}, 5671 $Å^3$ for Cu^{2+}, and 6218 $Å^3$ for Fe^{3+}. Moreover, the total interaction energies between the host matrix (ZrSPhP) and guest (cations) were calculated. The results suggest that the strength of the interactions decreases with the valency, thus, sodium cations are held the toughest. Both of these results are in agreement with the results of experimental treatment of the real samples with HCl when the content of the sodium cations in the intercalate did not change, while the copper cations' and yet more iron cations' content decreased.

4.5. Other results

Additionally to the previous research, the arrangement of methoxy-derivatives of APY2 (further denoted as moAPY2) within the layers of ZrSPhP was also studied as another potential material for optical applications. In this case, the compound has not yet been successfully synthesized experimentally, therefore it was unable to compare the results of the calculation with experimental data, like the diffraction pattern in the previous cases. Due to this difficulty, the calculations were focused only at comparison of different arrangements between each other with respect of the values of total potential energy.

For moAPY2, similarly to the APY2, various types of arrangements were prepared in the initial models. The experimental results for APY2 intercalate were used as the basic information about the structure – chemical composition (which did not differ a lot for other derivatives), protonation of the molecules, water content or

initial cell basal spacing. Different orientations of the rows of intercalated molecules along *a* and along *b* cell axis were built, see Fig. 17, and compared after geometry optimization and dynamics calculation. The calculation showed that both orientations of the rows, like in the middle of Fig. 17, were most favourable in the resultant model with the lowest value of the potential energy. Therefore it is possible to conclude that there is not one preferred orientation of the intercalated molecules based only on the comparison of potential energies. The optimized structure revealed more disordered arrangement of the intercalated molecules than in case of APY2 and can be compared to the results for NO2APY2 derivative intercalation, see Fig. 15. The dipole moments reached values around 107 Debye which is about 15 times higher values than in case of APY2 and 4 times higher than MeAPY2, yet lower than NO2APY2 derivative (193 Debye). This presumes that also moAPY2 derivative could be a good candidate for non-linear optical applications, similarly to NO2APY2.

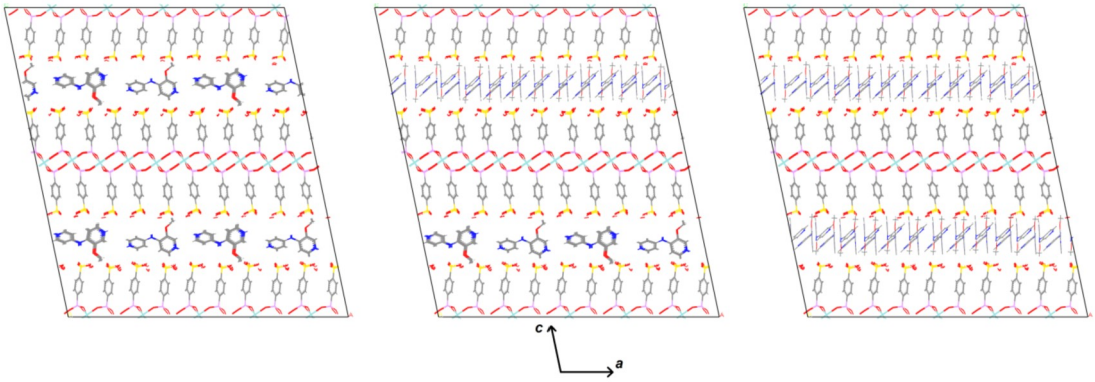

Fig. 17: Different orientations of guest molecules of moAPY2 in the initial models [71]

5. Conclusions

This thesis was aimed on the description of intercalated layered materials with partially disordered arrangements. For this purpose, the methods of classical molecular simulations were used with a combination of experimental results of X-ray diffraction, chemical analysis, infrared and UV spectroscopy and other methods. The calculations are suitable for the materials that are difficult or impossible to be prepared in a form for direct structural analysis. With a combination with experiments, the simulations can give us advice for preparation of new materials or support experimental results of the prepared samples.

The main compound that has been studied in this work was zirconium 4-sulfophenylphosphonate, a material with potential applications beside others in fuel cells thanks to its proton conductivity. Its geometry was only sketched before. At first, the non-intercalated structure of pure ZrSPhP was determined. Both fully and partially sulfonated models were optimized and its structure deduced. The influence of the position of the water molecules present in the structure and sulfonation of the phenyl rings on the resultant diffraction pattern was studied. The position of the water molecules was found to be along the planes of oxygen atoms of sulfo groups.

The knowledge of the fundamental structure of ZrSPhP served for further calculation of intercalated models. The arrangements of optically active molecules of APY2 and its methyl-, nitro- and methoxy- derivatives were investigated. For all types of the guest molecules, a disordered arrangement was obtained. For APY2 and NO2APY2 intercalates there was an evident partial row arrangement as a remainder of the arrangement in the initial models. Based on the calculations of the values of dipole moments of different guest molecules, NO2APY2, with the highest value, was selected as the most promising material for non-linear optics applications.

The intercalation of three cations with different valency Na^{+}, Cu^{2+} and Fe^{3+} between the layers of ZrSPhP was studied. The size, the amount and the charge of the intercalated cations played major role in their final arrangements in the interlayer space. In case of sodium, the cations replaced the positions of the water molecules and formed a sheet in a plane of the sulfo groups of ZrSPhP. The copper and iron cations were distributed with higher disorder in the middle of the interlayer space. The calculated interactions energies showed that the sodium cations are held with the

strongest interaction between the layers of the host while iron with the weakest one. This was confirmed by the experimental results of the exchange reactions.

6. References

[1] Clearfield, A.; Smith, S. D.: The Crystal Structure of Zirconium Phosphate and the Mechanism of Its Ion Exchange Behavior. *J. Colloid Interf. Sci.* **28** (1968), 325–330.

[2] Clearfield, A.; Smith, G. D.: The Crystallography and Structure of α-Zirconium Bis(monohydrogen orthophosphate) Monohydrate. *Inorg. Chem.* **8** (1969), 431–436.

[3] Troup, J. M.; Clearfield, A.: On the Mechanism of Ion Exchange in Zirconium Phosphates. 20. Refinement of the Crystal Structure of α-Zirconium Phosphate. *Inorg. Chem.* **16** (1977), 3311–3314.

[4] Alberti, G.; Costantino, U.; Allulli S.; Tomassini N.: Crystalline $Zr(R\text{-}PO_3)_2$ and $Zr(R\text{-}OPO_3)_2$compounds (R = organic radical): A new class of materials having layered structure of the zirconium phosphate type. *J. Inorg. Nucl. Chem.* **40** (1978), 1113–1117.

[5] Poojary, M. D.; Hu, H.-L.; Campbell III, F. L.; Clearfield, A.: Determination of Crystal Structures from Limited Powder Data Sets: Crystal Structure of Zirconium Phenylphosphonate. *Acta Crystallogr.* B **49** (1993), 996–1001.

[6] Curini, M.; Rosati, O.; Costantino, U.: Heterogeneous Catalysis in Liquid Phase Organic Synthesis, Promoted by Layered Zirconium Phosphates and Phosphonates. *Curr. Org. Chem.* **8** (2004), 591–606.

[7] Newman, S. P.; Jones, W.: Synthesis, characterization and applications of layered double hydroxides containing organic guests. *New J. Chem.* **22** (1998), 105–115.

[8] Ulibarri, M. A.; Pavlovic, I.; Barriga, C.; Hermosín, M. C.; Cornejo, J.: Adsorption of anionic species on hydrotalcite-like compounds: effect of interlayer anion and crystallinity. *Appl. Clay Sci.* **18** (2001), 17–27.

[9] Mallouk, T. E.; Gavin, J. A.: Molecular Recognition in Lamellar Solids and Thin Films. *Acc. Chem. Res.* **31** (1998), 209-217.

[10] Palacín, M. R.: Recent advances in rechargeable battery materials: a chemist's perspective. *Chem. Soc. Rev.* **38** (2009), 2565–2575.

[11] Carrado, K. A.: Synthetic organo- and polymer–clays: preparation, characterization, and materials applications. *Appl. Clay Sci.* **17** (2000), 1–23.

[12] Chen, B.; Evans, J. R. G.; Greenwell, H. C.; Boulet, P.; Coveney, P. V.; Bowden, A. A.; Whiting, A.: A critical appraisal of polymer–clay nanocomposites. *Chem. Soc. Rev.* **37** (2008), 568–594.

[13] Choy, J.-H.; Choi, S.-J.; Oh, J.-M.; Park, T.: Clay minerals and layered double hydroxides for novel biological applications. *Appl. Clay. Sci.* **36** (2007), 122–132.

[14] Cao, G.; Lee, H.; Lynch, V. M.; Mallouk, T. E.: Synthesis and Structural Characterization of a Homologous Series of Divalent-Metal Phosphonates, $M^{II}(O_3PR)\cdot H_2O$ and $M^{II}(HO_3PR)_2$. *Inorg Chem.* **27** (1988), 2781–2785.

[15] Clearfield, A.; Blessing, R. H.; Stynes, J. A.: New Crystalline Phases of Zirconium Phosphate Possessing Ion-Exchange Properties. *J. Inorg. Nucl. Chem.* **30** (1968), 2249–2258.

[16] Rajeh, A. O.; Szirtes L.: Investigations of Crystalline Structure of Gamma-Zirconium Phosphate. *J. Radioanal. Nucl. Ch. Ar.* **195** (1995), 319–322.

[17] Poojary, D. M.; Shpeizer, B.; Clearfield, A.: X-Ray Powder Structure and Rietveld Refinement of γ-Zirconium Phosphate, $Zr(PO_4)(H_2PO_4)\cdot 2H_2O$. *J. Chem. Soc. Dalton* (1995), 111–113.

[18] Poojary, D. M.; Zhang, B.; Clearfield, A.: Synthesis and Crystal Structure of a New Layered Zirconium Phosphate Compound, $Zr(PO_4)F(OSMe_2)$. *J. Chem. Soc. Dalton* (1995), 2453–2456.

[19] Clearfield, A.; Demadis, K.: Metal Phosphonate Chemistry: From Synthesis to Applications. Royal Society of Chemistry, Cambridge, 2012.

[20] Clearfield, A.; Stynes, J. A.: The Preparation of Crystalline Zirconium Phosphate and Some Observations on Its Ion Exchange Behaviour. *J. Inorg. Nucl. Chem.* **26** (1964), 117-129.

[21] Alberti, G.; Costantino, U.; Giovagnotti, M. L. L.: Synthesis and ion-exchange properties of zirconium bis-(carboxymethanephosphonate), a new organic-inorganic ion exchanger. *J. Chromatogr. A* **180** (1979), 45–51.

[22] Burwell, D. A.; Thompson, M. E.: Synthesis of layered $Zr(O_3PCH_2CH_2COCl)_2$ from $Zr(O_3PCH_2CH_2COOH)_2$. *Chem. Mater.* **3** (1991), 14–17.

[23] Burwell, D. A.; Thompson, M. E.: Synthesis of amide- and ester-functionalized zirconium phosphonates. *Chem. Mater.* **3** (1991), 730–737.

[24] Környei, J.; Szirtes, L.; Costantino, U.: Intercalation behaviour of organic derivatives of alpha-zirconium phosphate. *J. Radioanal. Nucl. Ch.* **89** (1985), 331–338.

[25] Casciola, M.; Costantino, U.; Peraio, A.; Rega, T.: Zirconium 2-amino ethyl phosphonate:preparation, characterization and preliminary study of its electrical conductivity and intercalation properties. *Solid State Ionics* **77** (1995), 229–233.

[26] Tsai, T. Y.; Wu, Y. J.; Hsu, F. J.: Synthesis and properties of epoxy/layered zirconium phosphonate (Zr-P) nanocomposites. *J. Phys. Chem. Solids* **69** (2008), 1379–1382.

[27] Yang, C.-Y.; Clearfield, A.: The preparation and ion-exchange properties of zirconium sulphophosphonates. *React. Polym.* **5** (1987), 13–21.

[28] Alberti, G.; Casciola, M.; Costantino, U.; Peraio, A.; Montoneri, E.: Protonic conductivity of layered zirconium phosphonates containing $–SO_3H$ groups. I. Preparation and characterizationof a mixed zirconium phosphonate of composition $Zr\ (O_3PR)_{0.73}(O_3PR')_{1.27}\cdot nH20$, with R =$–C_6H_4–SO_3H$ and R' = $–CH_2–OH$. *Solid State Ionics* **50** (1992), 315–322.

[29] Alberti, G.; Casciola, M.; Palombari, R.; Peraio, A.: Protonic conductivity of layered zirconium phosphonates containing $–SO_3H$ groups. II. Ac conductivity of zirconium alkyl-sulphophenyl phosphonates in the range 100–200°C, in the presence or absence of water vapour. *Solid StateIonics* **58** (1992), 339–344.

[30] Stein, E. W.; Clearfield, A.; Subramanian, M. A.: Conductivity of group IV metal sulfophosphonates and a new class of interstratified metal amine-sulfophosphonates. *Solid State Ionics* **83** (1996), 113–124.

[31] Alberti, G.; Casciola, M.; Dannadio, A.; Piaggio, P.; Pica, M.; Sisani, M.: Preparation and characterisation of α-layered zirconium phosphate sulfophenylenphosphonates with variable concentration of sulfonic groups. *Solid State Ionics* **176** (2005), 2893–2898.

[32] Zima, V.; Svoboda, J.; Melánová, K.; Beneš, L.; Casciola, M.; Sganappa, M.; Brus, J.; Trchová, M.: Synthesis and characterization of new zirconium 4-sulfophenylphosphonates. *Solid State Ionics* **181** (2010), 705–710.

[33] Svoboda, J.; Zima, V.; Melánová, K.; Beneš, L.; Trchová, M.: Intercalation chemistry of zirconium 4-sulfophenylphosphonate. *J. Solid State Chem.* **208** (2013), 58–64.

[34] Rao, V.; Kluy, N.; Ju, W.; Stimming, U.: Proton-Conducting Membranes for Fuel Cells. In: Handbook of Membrane Separations: Chemical, Pharmaceutical, Food, and Biotechnological Applications, Second Edition. CRC Press, 2015.

[35] Montoneri, E.; Viscardi, G.; Bottigliengo, S.; Chierotti, M. R.; Buscaino, R.; Quaglitto, P.: 4-Sulfophenylphosphonic Acid: A Novel Precursor to Fabricate Polyfunctional Acid Materials. *Chem. Mater.* **19** (2007), 2671–2678.

[36] Maniam, P.; Näther, C.; Stock, N.: Systematic hydrothermal investigation of metal phosphonatobenzenesulfonates by high-throughput methods. *Eur. J. Inorg. Chem.* **2010** (2010), 3866–3874.

[37] Maniam, P.; Stock, N.: A three-dimensional tin(II) phosphonatobenzenesulfonate with Sn_4O_{12} clusters. *Acta Crystallogr C* **67** (2011), M73–M76.

[38] Maniam, P.; Stock, N.: Synthesis and Characterization of the Mixed-Linker Copper(II) Coordination Polymer $[Cu(HO_3PC_6H_4SO_3)(C_{10}N_2H_8)]\cdot H_2O$. *Anorg Allg Chem* **637** (2011), 1145–1151.

[39] Du, Z. Y.; Huang, J.-J.; Xie, Y.-R.; Wen, H.-R.: Two new 1D structures of copper(II) or yttrium(III) phosphonatobenzenesulfonates using 1,10-phenanthroline as auxilary ligang. *J. Mol. Struct.* **919** (2009), 112–116.

[40] Jacobson, A. J.: Intercalation reaction of layered compounds. In: Solid state chemistry compounds, eds.: Cheetham, A. K.; Day, P., Clarendon Press, Oxford, 1992, p. 182, chapter 6.

[41] Kanis, D. R.; Ratner, M. A.; Marks, T. J.: Design and Construction of Molecular Assemblies with Large Second-Order Optical Nonlinearities. Quantum Chemical Aspects. *Chem. Rev.* **94** (1994), 195–242.

[42] He, G. S.; Tan, L.-S.; Zheng, Q.; Prasad, P. N.: Multiphoton Absorbing Materials: Molecular Designs, Characterizations, and Applications. *Chem. Rev.* **108** (2008), 1245–1330.

[43] Bureš, F.; Cvejn, D.; Melánová, K.; Beneš, L.; Svoboda, J.; Zima, V.; Pytela, O.; Mikysek, T.; Růžičková, Z.; Kityk, I. V.; Wojciechowski, A.; AlZayed, N.: Effect of intercalation and chromophore arrangement on the linear and nonlinear optical properties of model aminopyridine push-pull molecules. *J. Mater. Chem. C* **4** (2016), 468–478.

[44] Franken, P. A.; Hill, A. E.; Peters, C. W.; Weinreich, G.: Generation of Optical Harmonics. *Phys. Rev. Lett.* **7** (1961), 118-120.

[45] Kovář, P.; Škoda, J.; Pospíšil, M.; Melánová, K.; Svoboda, J.; Beneš L.; Kutálek, P.; Zima, V.; Bureš, F.: How *N*-(pyridin-4-yl)pyridin-4-amine and its methyl and nitro derivatives are arranged in the interlayer space of zirconium sulfophenylphosphonate: solved by experimental and calculation methods. Submitted in 2019.

[46] Terban, M. W.; Shi, C.; Silbernagel, R.; Clearfield, A.; Billinge S. J. L.: Local Environment of Terbium(III) Ions in Layered Nanocrystalline Zirconium(IV) Phosphonate-Phosphate Ion Exchange Materials. *Inorg. Chem.* **56** (2017), 8837–8846.

[47] Chmielarz, L.; Piwowarska, Z.; Kuśtrowski, P.; Węgrzyn, A.; Gil, B.; Kowalczyk, A.; Dudek, B.; Dziembaj, R.; Michalik, M.: Comparison Study of Titania Pillared Interlayered Clays and Porous Clay Heterostructures Modified with Copper and Iron as Catalysts of The DeNOx Process. *Appl. Clay Sci.* **53** (2011), 164–173.

[48] Zehhaf, A.; Morallon, E.; Benyoucef, A.: Polyaniline/Montmorillonite Nanocomposites Obtained by In Situ Intercalation and Oxidative Polymerization in Cationic Modified-Clay (Sodium, Copper and Iron). *J. Inorg. Organomet. Polym.* **23** (2013), 1485–1491.

[49] Melánová, K.; Beneš, L.; Svoboda, J.;, Zima, V.; Trchová, M.; Vlček, M.; Almonasy, N.: Cerium(IV) phenylphosphonates and para-substituted phenylphosphonates: preparation and characterization. *J. Incl. Phenom. Macrocycl. Chem.* **87** (2017), 331–339.

[50] Rappé, A. K.; Casewit, C. J.; Colwell, K. S.; Goddard, W. A. III; Skiff, W. M.: UFF, a full periodic table force field for molecular mechanics and molecular dynamics simulations. *J. Am. Chem. Soc.* **114** (1992), 10024–10039.

[51] Dauber-Osguthorpe, P.; Roberts, V. A.; Osguthorpe, D. J.; Wolff, J.; Genest, M.; Hagler, A. T.: Structure and energetics of ligand binding to proteins: E. coli dihydrofolate reductase-trimethoprim, a drug-receptor system. *Proteins*, **4** (1988), 31–47.

[52] Cornell, W. D.; Cieplak, P.; Bayly C. I.; Gould, I. R.; Merz, K. M.; Ferguson, D. M.; Spellmeyer, D. C.; Fox T.; Caldwell, J. W.; Kollman P. A.: A Second Generation Force Field for the Simulation of Proteins, Nucleic Acids, and Organic Molecules. *J. Am. Chem. Soc.*, **117** (1995), 5179–5197.

[53] Mayo, S. L.; Olafson, B. D.; Goddard, W. A. III: DREIDING: A generic force field for molecular simulations. *J. Phys. Chem.* **94** (1990), 8897–8909.

[54] Hwang, M. J.; Stockfisch, T. P.; Hagler, A. T.: Derivation of Class II Force Fields. 2. Derivation and Characterization of a Class II Force Field, CFF93, for the Alkyl Functional Group and Alkane Molecules. *J. Am. Chem. Soc.* **116** (1994), 2515–2525.

[55] Huai, S.; Mumby, S. J.; Maple, J. R.; Hagler, A. T.: An ab Initio CFF93 All-Atom Force Field for Polycarbonates. *J. Am. Chem. Soc.* **116** (1994), 2978–2987.

[56] Sun, H.: COMPASS: An ab Initio Force-Field Optimized for Condensed-Phase Applications – Overview with Details on Alkane and Benzene Compounds. *J. Phys. Chem. B* **102** (1998), 7338–7364.

[57] Karasawa, N.; Goddard, W. A. III: Acceleration of Convergence for Lattice Sums. *J. Phys. Chem.* ***93*** (1989), 7320–7327.

[58] Materials Studio Modeling Environment, Release 4.3 Documentation. Accelrys Software Inc., San Diego, CA, 2003.

[59] Polak, E.; Ribière, G.: Note sur la convergence de directions conjugu´ee. *Rev. Fr. Inform. Rech. O.* **16** (1969), 35–43.

[60] Fletcher, R.; Reeves, C. M.: Function Minimization by Conjugate Gradients. *Comput. J.* **7** (1964), 149–154.

[61] Tolman, R. C.: The Principles of Statistical Mechanics. Oxford University Press, Oxford, 1938.

[62] Berendsen, H. J. C.; Postma, J. P. M.; van Gunsteren, W. F.; DiNola, A.; Haak, J. R.: Molecular dynamics with coupling to an external bath. *J. Chem. Phys.* **81** (1984), 3684–3690.

[63] Nosé, S.: Constant temperature molecular dynamics methods. *Prog. Theor. Phys. Supp.* **103** (1991), 1–46.

[64] Andersen, H. C.: Molecular dynamics simulations at constant pressure and/or temperature. *J. Chem. Phys.* **72** (1980), 2384–2393.

[65] Parrinello, M.; Rahman, A.: Polymorphic transitions in single crystals: A new molecular dynamics method. *J. Appl. Phys.* **52** (1981), 7182–7190.

[66] Giacovazzo, C. (ed.): Fundamentals of Crystallography. Oxford University Press, Oxford, 2000.

[67] Rappé, A. K.; Goddard, W. A. III: Charge Equlibration for Molecular Dynamics Simulations. *J. Phys. Chem.* **95** (1991), 3358–3363.

[68] Čapková, P.; Beneš, L.; Melánová, K.; Schenk, H.: Structure analysis of intercalated zirconium phosphate using molecular simulation. *J. Appl. Crystallogr.* **31** (1998), 845–850.

[69] Škoda, J.; Pospíšil, M.; Kovář, P.; Melánová, K.; Svoboda, J.; Beneš L.; Zima, V.: How Intercalated Sodium, Copper, and Iron Cations Influence the Structural Arrangement of Zirconium Sulfophenylphosphonate Layers? Theoretical and Experimental Points of View. *J. Phys. Chem. C*, **123** (2019), 2488–2495.

[70] Škoda, J.; Pospíšil, M.; Kovář, P.; Melánová, K.; Svoboda, J.; Beneš L.; Zima, V.: Geometry optimization of zirconium sulfophenylphosphonate layers by molecular simulation methods. *J. Mol. Model.*, **24** (2018), 1–12.

[71] Škoda, J.; Pospíšil, M.; Kovář, P.: Study of optically active 3 methoxy-*N*-(pyridin-4-yl)pyridin-4-amine intercalated into zirconium 4-sulfophenylphosphonate layers by molecular simulation methods. *Materials Structure*, submitted in 2019.

7. Acknowledgements

This work was supported by:

Czech Science Foundation Projects No. 14-13368S

Czech Science Foundation Projects No. 17-10639S

Charles University project SVV260 443 "Studentský výzkum v oboru biofyzika a chemická fyzika"

8. List of abbreviations

- *α*-ZrP – α-zirconium bis-(monohydrogen orthophosphate) monohydrate
- APY2 – *N*-(pyridin-4-yl)pyridin-4-amine
- MeAPY2 – 3-methyl-*N*-(pyridin-4-yl)pyridin-4-amine
- moAPY2 – 3-methoxy-*N*-(pyridin-4-yl)pyridin-4-amine
- NO2APY2 – 3-nitro-*N*-(pyridin-4-yl)pyridin-4-amine
- XRD – X-ray diffraction
- ZrSPhP – zirconium 4-sulfophenylphosphonate
- ZrSPhP0.7 – $Zr(HO_3SC_6H_4PO_3)_{0.7}(C_6H_5PO_3)_{1.3}\cdot yH_2O$
- ZrSPhP1.3 – $Zr(HO_3SC_6H_4PO_3)_{1.3}(C_6H_5PO_3)_{0.7}\cdot yH_2O$
- ZrSPhP2 – $Zr(HO_3SC_6H_4PO_3)_2\cdot yH_2O$

9. List of Figures

10. List of publications and scientific contributions

Articles in impacted journals

- Škoda, J.; Gabriel, P.; Dienstbier, M.: Světelná degradace piva a tvorba letinkové příchuti. *Chem. Listy*, **110** (2016), 112–117.

- Škoda, J.; Pospíšil, M.; Kovář, P.; Melánová, K.; Svoboda, J.; Beneš, L.; Zima V.: Geometry Optimization of Zirconium Sulfophenylphosphonate Layers by Molecular Simulation Methods. *J. Mol. Model*. **24** (2018) 10.

- Škoda, J.; Pospíšil, M.; Kovář, P.; Melánová, K.; Svoboda, J.; Beneš, L.; Zima, V.: How Intercalated Sodium, Copper, and Iron Cations Influence the Structural Arrangement of Zirconium Sulfophenylphosphonate Layers? Theoretical and Experimental Points of View. *J. Phys. Chem. C.*, **123** (2019) 2488–2495.

- Kovář, P.; Škoda, J.; Pospíšil, M.; Melánová, K.; Svoboda, J.; Beneš, L.; Kutálek, P.; Zima, V.; Bureš, F.: How *N*-(pyridin-4-yl)pyridin-4-amine and its methyl and nitro derivatives are arranged in the interlayer space of zirconium sulfophenylphosphonate: solved by experimental and calculation methods. Submitted in 2019.

Articles in recensed journals

- Škoda, J.; Pospíšil, M.; Kovář, P.: Study of optically active 3-methoxy-*N*-(pyridin-4-yl)pyridin-4-amine intercalated into zirconium 4-sulfophenylphosphonate layers by molecular simulation methods. *Materials Structure*, submitted in 2019.

Other contributions

- Škoda, J., Pšenička, M., Pospíšil, M.: Structural analysis of layered double hydroxides intercalated by drugs by the methods of molecular simulations. *Informátor* of Czech Clay Group, **64** (2019), 1–4, ISSN: 1802-249.

Abstracts and conference contributions

- Week of doctoral students, 2015, Prague, Czech Republic, poster and oral contribution – "Molecular simulations of Zr derivatives containing sulfophenylphosphonates", Škoda J., Pospíšil M., Melánová K.

- V. International Workshop On Layered Materials, Třešť, Czech Republic, 15.–19. 9. 2015, poster contribution in English and abstract – "Molecular simulations of Zr derivatives containing sulfophenylphosphonates", Škoda J., Pospíšil M.

- School on Layered Materials, Prague, Czech Republic, 21.–22. 3. 2016, poster contribution in English and abstract – "Optimized structures of zirconium sulfophenylphosphonates – molecular simulations study", Škoda J., Pospíšil M., Melánová K.

- 8th Mid-European Clay Conference, 4.8. 7. 2016 Košice, Slovakia, poster presentation – "Interlayer structures of zirconium phosphonates with sulfophenyl and phenyl groups solved by molecular modelling methods, Škoda J., Pospíšil M., Melánová K., best student poster award

- VI. International Workshop On Layered Materials, Kutná Hora, Czech Republic, 5.–9. 9. 2016, poster contribution in English – "Zirconium phosphonate derivatives intercalated with sodium cations – molecular modelling study", Škoda J., Pospíšil M., Kovář P., Melánová K.

- International Workshop On Layered Materials, Třešť, Czech Republic, 1.–5. 9. 2017, poster contribution and abstract – "Molecular simulation of the crystal structure of Zr phosphonate intercalated with 4-4'-dipyridylamine derivatives", Škoda J., Pospíšil M., Kovář P., Zima V., Melánová K.

- 7th International Workshop on Layered Materials, Kraków-Tomaszowice, Poland, 9.–13. 9. 2018:

- oral contribution in English and abstract – “Zirconium sulfophenyl phosphonates intercalated with organic species and cations”, Škoda J., Pospíšil M., Kovář P., Zima V., Melánová K., Beneš L., Svoboda J.;
- poster presentation in English and abstract – “Clay minerals intercalated with drugs described by molecular modelling”, Škoda J., Pšenička M., Pospíšil M.;
- poster contribution – “Structural arrangement of zirconium sulfophenylphosphonate layers intercalated with Na^{+}, Cu^{2+} and Fe^{3+} cations”, Zima V., Škoda J., Pospíšil M., Kovář P., Melánová K., Svoboda J., Beneš L.

- Seminar of Czech National Clay Group, Prague, Czech Republic, 30. 11. 2018, oral contribution in Czech – “Structural analysis of layered double hydroxides intercalated with drugs by molecular simulation methods”, Škoda J., Pšenička M., Pospíšil M.

- Seminar of the Department of Chemical Physics and Optics, Prague, Czech Republic, 14. 3. 2019, oral contribution in English – “Zirconium sulfophenyl phosphonates intercalated with organic species and cations”, Škoda J., Pospíšil M., Kovář P., Zima V., Melánová K., Beneš L., Svoboda J.

- Struktura 2019, crystallographic colloquium, Žďár nad Sázavou, Czech Republic, 10.–13. 6. 2019, oral contribution in English – “Study of the arrangement of intercalated organic species within layered materials by molecular simulation methods”, Škoda J., Pšenička M., Kovář P., Pospíšil M.

- Euroclay 2019, Paris, France, 1.–5. 7. 2019, poster contribution – “Sulindac and Mefenamic acid intercalated into LDHs described by combination of DFT and classical MD simulations”, Pšenička M., Škoda J., Pospíšil M.

11. Attachments – articles